WYOMING STATE GEOLOGICAL SURVEY
Thomas A. Drean, Director and State Geologist
Laramie, Wyoming

Geology - Interpreting the past - Providing for the future

OPEN FILE REPORT 14-2
Mc Intosh Meadows 1:24,000-scale
Bedrock Geologic Map

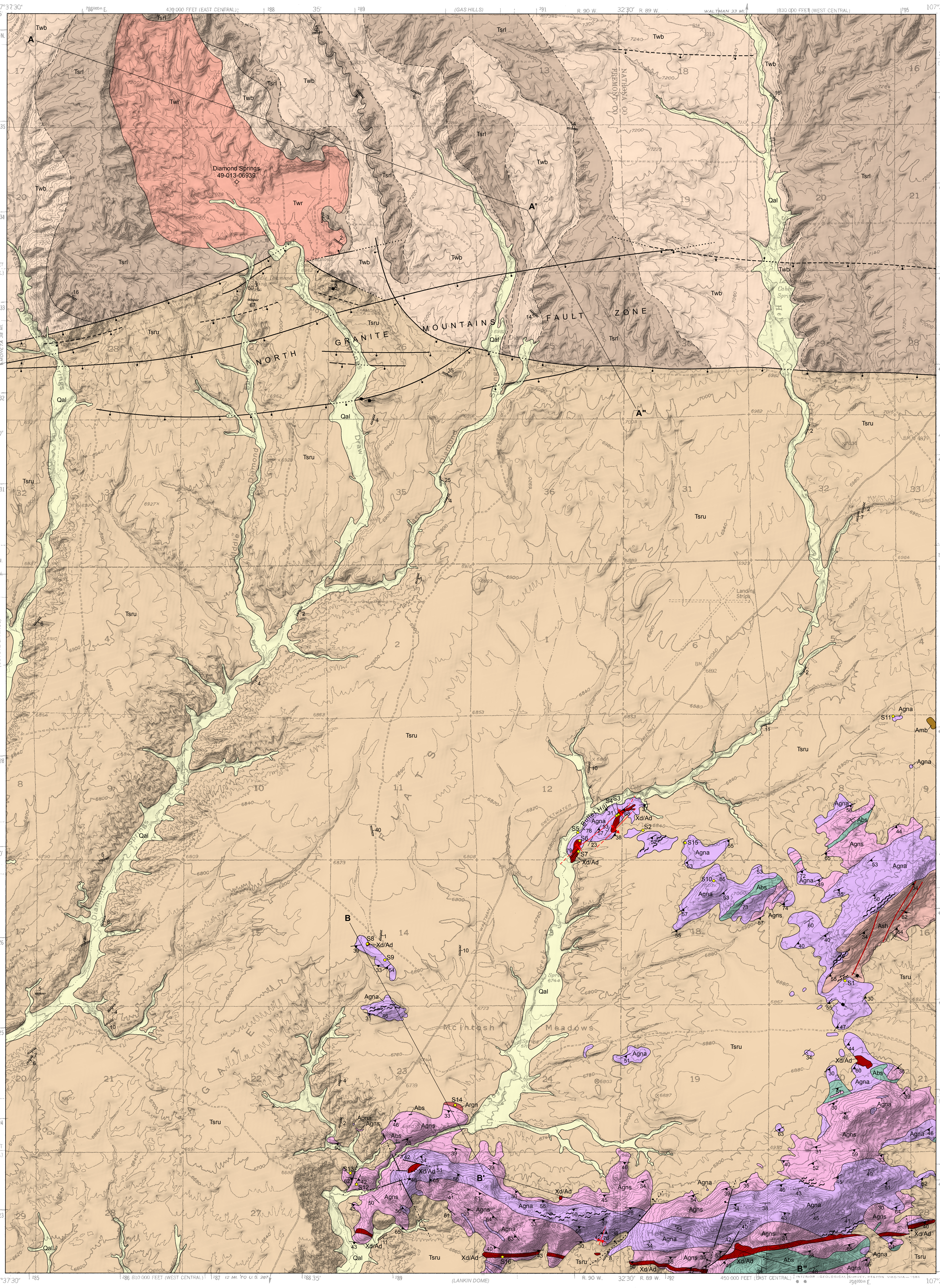

Base map from U.S. Geological Survey 1:24,000-scale topographic map of the Mc Intosh Meadows, Wyoming Quadrangle, 1952, photorevised 1984

Base hillshade derived from USDA/NRCS – National Cartography & Geospatial Center 10-meter Digital Elevation Model (DEM), 2000; azimuth 315º, sun angle 45º, vertical exaggeration 2

Projection: Universal Transverse Mercator (UTM), zone 13
North American Datum of 1927 (NAD 27)
1,000-meter grid ticks: UTM, zone 13
10,000-foot grid ticks: Wyoming State Plane Coordinate System, west central and east central zones

Wyoming State Geological Survey
P.O. Box 1347 - Laramie, WY 82073-1347
Phone: 307-766-2286 - Fax: 307-766-2605
Email: wsgs.sales@wyo.gov

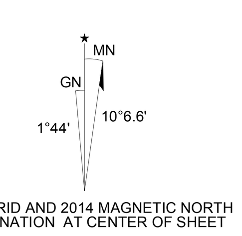

UTM GRID AND 2014 MAGNETIC NORTH DECLINATION AT CENTER OF SHEET

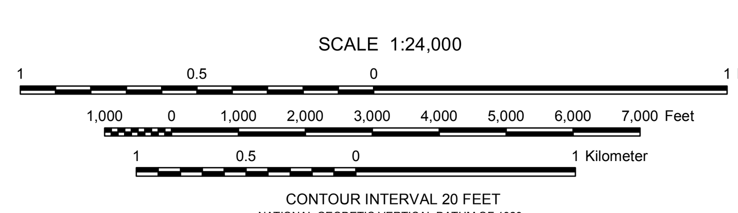

CONTOUR INTERVAL 20 FEET
NATIONAL GEODETIC VERTICAL DATUM OF 1929

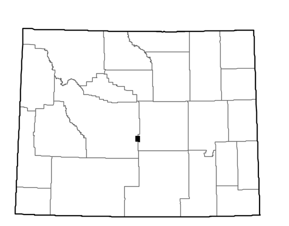

WYOMING QUADRANGLE LOCATION

Digital cartography by Elizabeth C. Cola

Map edited by Suzanne C. Luhr

Prepared in cooperation with and research supported by the U.S. Geological Survey, National Cooperative Geologic Mapping Program, under USGS award number G13AC000234. The views and conclusions contained in this document are those of the authors and should not be interpreted as necessarily representing the official policies, either expressed or implied, of the U.S. Government.

PRELIMINARY GEOLOGIC MAP OF THE MC INTOSH MEADOWS QUADRANGLE, FREMONT AND NATRONA COUNTIES, WYOMING

by

Elizabeth C. Cola and Wayne M. Sutherland

2014

EXPLANATION

CORRELATION OF MAP UNITS
(* indicates a formation only shown in cross section)

Unit	Epoch	Period	Era
Qal	Holocene	QUATERNARY	CENOZOIC
Unconformity			
Tsru, Tsrs*, Tsrc*, Tsrl	Miocene	TERTIARY	CENOZOIC
Unconformity			
Twr	Oligocene	TERTIARY	CENOZOIC
Unconformity			
Twb	Eocene	TERTIARY	CENOZOIC
Unconformity			
Czr*	Paleocene	TERTIARY	CENOZOIC
Unconformity			
Mzr*	Cretaceous Jurassic Triassic	CRETACEOUS JURASSIC TRIASSIC	MESOZOIC
Unconformity			
Xd/Ad	Proterozoic	PROTEROZOIC	PRECAMBRIAN
Argn, Ash	Neoarchean	ARCHEAN	PRECAMBRIAN
Amb, Abs	Mesoarchean	ARCHEAN	PRECAMBRIAN
Agns, Agna	Paleoarchean	ARCHEAN	PRECAMBRIAN

DESCRIPTION OF MAP UNITS
(*indicates unit only shown in cross section)

Cenozoic

Qal — **Alluvium (Holocene)**—Unconsolidated clay, silt, sand, gravel, and cobbles located in and along most drainages; may include eluvial deposits, slope wash, and small alluvial and colluvial fans along drainages

Split Rock Formation (Miocene)

Tsru — **Upper porous sandstone sequence**—As much as 305 m (1000 ft) thick with resistant coarse, crossbedded conglomerate that persistently caps hills and buttes underlain by white to cream and tan, very fine to fine-grained, tuffaceous sandstone and ash layers south of the North Granite Mountains Fault; Sweetwater agates found in residuum help to distinguish between adjacent outcrops of similar lithologies in the Split Rock Formation and those in the Wagon Bed Formation

Tsrs* — **Silty sandstone sequence***—As much as 183 m (600 ft) thick buff to white fine-grained sandstone interbedded with tuff and pumicite. A silty matrix within the sandstone is common throughout this unit, as is the presence of abundant glass shards (Love, 1970). This was only exposed in one outcrop, too small to show, along East Diamond Springs Creek in the SW¼ SE¼ NE¼, Sec. 35, T32N, R90W

Tsrc* — **Clayey sandstone sequence***—30 to 91 m (100 to 300 ft) thick composed almost entirely of a gray, fine- to medium-grained, very soft clayey sandstone; fines upward and contains bentonitic beds, quartz bipyramids, and glass shards; thins toward Precambrian rocks

Tsrl — **Lower porous sandstone sequence**—As much as 152m (500 ft) of poorly exposed pebble and cobble conglomerate within a mudstone matrix, well-rounded, well-sorted volcanic sandstone, and local beds of gray vitric tuff; unconformably overlies the Wagon Bed Formation

Twr — **White River Formation (Oligocene)**—76 m (250 ft) or more of basal gray arkosic sandstone conglomerate that grades upward into massive, cliff-forming, white to grayish-orange, fine-grained, silty sandstone, hard siltstone, and claystone; thin beds of white tuff present throughout; unconformably overlies the Wagon Bed Formation with as much as 76 m (250 ft) of relief (Van Houten, 1964); present as channel fill in northwest part of map

Twb — **Wagon Bed Formation (middle and upper Eocene)**—Approximately 183 m (600 ft) of crossbedded conglomerates, sandstones, ash layers, and coarse lapilli tuff; conglomerates vary from dominantly Precambrian debris to volcanic with clasts exceeding 3 m (10 ft), ranging from angular to rounded in a matrix that varies from white to tan and rusty, fine- to coarse-grained arkosic sandstone, to cream silt and white ash; minor oil-soaked sandstone

Czr* — **Cenozoic rocks*, undivided**

Mesozoic

Mzr* — **Mesozoic rocks*, undivided**

Precambrian

Xd/Ad — **Mafic dike (Proterozoic and Neoarchean, undifferentiated)**—Diabase, amphibolite, or related mafic dikes of two ages occur within the map area and were not separated out during mapping. Older Archean dikes (>2.68 Ga; Grace and others, 2006) tend to be boudinaged and discontinuous as compared to similarly oriented younger dikes (2.115 Ga; K.R. Chamberlain, oral commun., Sept. 2014) that are near-vertical, relatively straight, uniform in thickness, and predominately trend east-northeast (Chamberlain and others, 2000)

Argn — **Red gneiss (?)**—Unknown age and origin, pink-red, felsic, medium- to coarse-grained; appears both unfoliated and pegmatitic, and foliated and gneissic within the same outcrop.

Ash — **East Sage Hen granite (Neoarchean)**—Pink- to orange-weathering, medium- to coarse-grained, unfoliated to weakly foliated, biotite granite dated by Langstaff (1995) to have a minimum crystallization U/Pb age of 2,622 ± 7 Ma, with a maximum projected at 2,650 Ma; extensively sheared

Rattlesnake Hills Group

Amb — **McDougal Gulch Metavolcanics (Mesoarchean)**—Amphibolite gneisses dominantly representative of metabasalts above the Barlow Springs Formation

Barlow Gap Group

Abs — **Barlow Springs Formation (Mesoarchean and Paleoarchean)**—Includes quartzite, metapelite, banded iron formation, metafelsite, and amphibolite gneiss; detrital zircon in quartzite was dated about 3,300 Ma (Langstaff, 1995); ages for metadacite near the formation top indicate 2,856 ± 55 Ma (Langstaff, 1995) and 2,864 ± 7.8 Ma (Fruchey, 2002); the Barlow Springs Formation is the base of supracrustal units on top of the metaigneous basement complex

Basement Gneiss Complex

Agns — **Sacawee orthogneiss (Paleoarchean)**—A distinctive coarse- to medium-grained, pink to tan, granitic-appearing, porphyritic gneiss with generally strong foliation characterized by large potassium feldspar crystals; foliation is defined by parallelism of biotite plates, and best observed where biotite is abundant (Bickford, 1977); age of 3,258 ± 8 Ma (Fruchey, 2002)

Agna — **Antler orthogneiss (Paleoarchean)**—Bodies of gray, fine-grained, finely layered, equigranular gneiss and quartzite layers within or adjacent to the Sacawee orthogneiss; foliation defined by alignment of biotite (Fruchey, 2002); dated at 3,370 ± 12 Ma from an outcrop east of the quadrangle (Langstaff, 1995) and dated within the quadrangle during this study in a fine-grained gneiss at ca. 3,325 Ma and a bluish-black quartzite at ca. 3.3 Ga (see written report for details)

MAP SYMBOLS

Definitions
Certain—Location known <25 m
Approximate—Estimated location 25–100 m
Inferred—Estimated location >100 m

Formation contact—Continuous where certain; short dash where inferred

Fault—Continuous where certain; long dash where approximately located; short dash where inferred; dotted where concealed; ball and bar on downthrown block of normal fault

Shear zone

Mafic dike

Synform—Continuous where certain; short dash where inferred

Antiform—Continuous where certain; short dash where inferred

A — A' **Line of cross section**

26 **Strike and dip of inclined bedding in crossbedded rocks**

15 **Strike and dip of inclined bedding**—Top direction unknown

Strike of vertical bedding—Top direction unknown

68 **Strike and dip of joint**

Strike of vertical joint

50 **Strike and dip of foliation**

S1 **Rock sample location**—Showing sample name (refer to accompanying report for analyses)

Diamond Springs 49-013-06939 **Dry hole**—Showing well name and API number

MAP REFERENCES

Bickford, F.E., 1977, Petrology and structure of the Barlow Gap area, Wyoming: Laramie, University of Wyoming, M.S. thesis, 76 p., scale 1:24,000.

Chamberlain, K.R., and Frost, B.R., 1995, Mid-Proterozoic mafic dikes in the central Wyoming Province: Evidence for Belt-age extension and supercontinent breakup: Geological Association of Canada–Mineralogical Association of Canada annual conference, Abstracts, v. 20, p. A-15.

Chamberlain, K.R., Sears, J.W., Frost, B.R., and Doughty, P.T., 2000, Ages of Belt Supergroup deposition and intrusion of mafic dikes in the central Wyoming Province: evidence for extension at ca. 1.5 Ga and 1.37 Ga and potential piercing points for Rodinia reconstructions: Geological Society of America, Abstracts with Programs, v. 32, no. 7, p. A-319.

Fruchey, B.L., 2002, Archean supracrustal sequences of contrasting origin—the Archean history of the Barlow Gap area, northern Granite Mountains, Wyoming: Laramie, University of Wyoming, M.S. thesis, 178 p., scales 1:24,000 and 1:3,000.

Grace, R.L.B., Chamberlain, K.R., Frost, B.R., and Frost, C.D., 2006, Tectonic histories of the Paleoarchean to Mesoarchean Sacawee block and Neoarchean Oregon Trail structural belt of south-central Wyoming Province: Canadian Journal of Earth Sciences, v. 43, no. 10, p. 1445–1466.

Langstaff, G.D., 1995, Archean geology of the Granite Mountains: Golden, Colorado School of Mines, Ph.D. dissertation, 671 p., scale 1:24,000.

Love, J.D., 1961, Split Rock Formation (Miocene) and Moonstone Formation (Pliocene) in central Wyoming: U.S. Geological Survey Bulletin 1121-I, 39 p.

Love, J.D., 1970, Cenozoic geology of the Granite Mountains area, central Wyoming: U.S. Geological Survey Professional Paper 495-C, 154 p., 4 pls.

Sutherland, W.M., and Hausel, W.D., 2003, Geologic map of the Rattlesnake Hills 30' x 60' quadrangle, Fremont and Natrona Counties: Wyoming State Geological Survey Map Series 61, 28 p., scale 1:100,000.

Sutherland, W.M., and Worman, B.N., 2013, Preliminary geologic map of the Blackjack Ranch quadrangle, Natrona County, Wyoming: Wyoming State Geological Survey, Open File Report 13-3, 24 p., scale 1:24,000.

Van Houten, F.B., 1955, Volcanic-rich middle and upper Eocene sedimentary rocks northwest of Rattlesnake Hills, central Wyoming: U.S. Geological Survey Professional Paper 274-A, 14 p.

Van Houten, F.B., 1964, Tertiary geology of the Beaver Rim area, Fremont and Natrona Counties, Wyoming: U.S. Geological Survey Bulletin 1164, 99 p., 8 pls., scale 1:62,500.

DISCLAIMERS

NOTICE TO USERS OF INFORMATION FROM THE WYOMING STATE GEOLOGICAL SURVEY

NOTICE FOR OPEN FILE REPORTS PUBLISHED BY THE WSGS

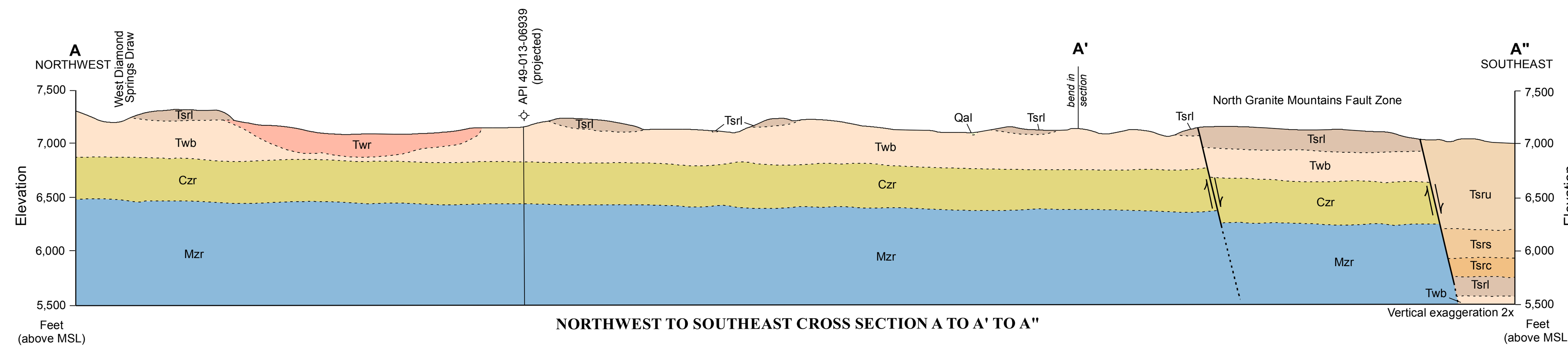

NORTHWEST TO SOUTHEAST CROSS SECTION A TO A' TO A''

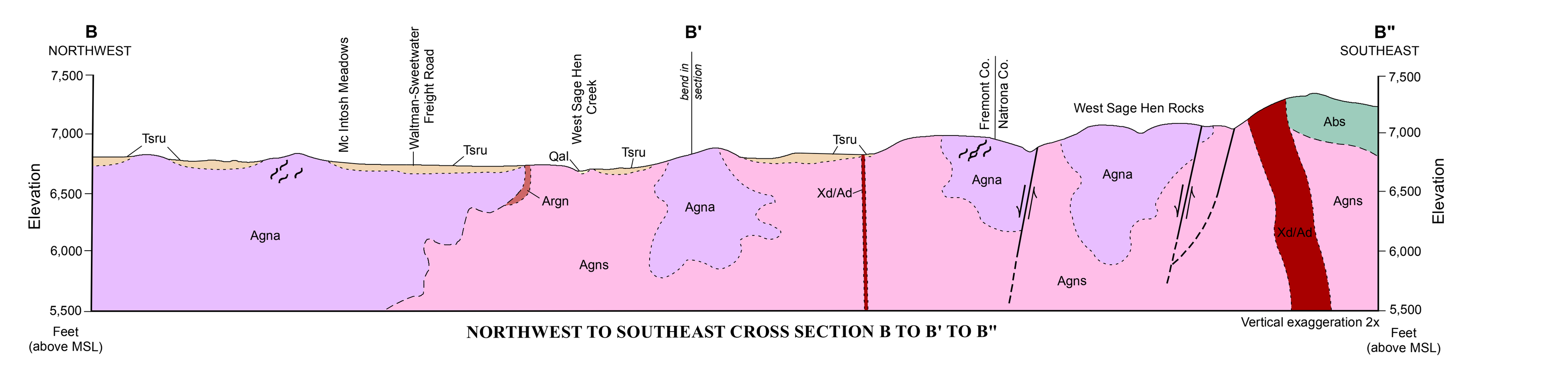

NORTHWEST TO SOUTHEAST CROSS SECTION B TO B' TO B''

WYOMING STATE GEOLOGICAL SURVEY
P.O. BOX 1347, LARAMIE, WY 82073
307-766-2286 • 307-766-2605 (fax)
wsgs.info@wyo.gov • www.wsgs.uwyo.edu
Director & State Geologist
Thomas A. Drean

Preliminary Geologic Map
of the
Mc Intosh Meadows 7.5' Quadrangle
Fremont and Natrona Counties, Wyoming

by

Elizabeth C. Cola and Wayne M. Sutherland

Open File Report 14-2
Laramie, Wyoming
September 12, 2014

Prepared in cooperation with and research supported by the U.S. Geological Survey, National Cooperative Geologic Mapping Program, under USGS award number G13AC000243. The views and conclusions contained in this document are those of the authors and should not be interpreted as necessarily representing the official policies, either expressed or implied, of the U.S. Government.

This report is preliminary and has not been reviewed for conformity with Wyoming State Geological Survey editorial standards or with the North American Stratigraphic Code.

Table of Contents

List of Figures

List of Tables

Preliminary Geologic Map
of the
Mc Intosh Meadows 7.5' Quadrangle
Fremont and Natrona Counties, Wyoming
Wyoming State Geological Survey Open File Report 14-2

By
Elizabeth C. Cola and Wayne M. Sutherland

Introduction

Recent exploration east of the Mc Intosh Meadows 7.5' quadrangle addressed gold, rare earth elements (REE), and iron. This economic interest indicated a need for remapping parts of the quadrangle and detailed mapping of the entire quadrangle. This map was completed in cooperation with the U.S. Geological Survey 2013 STATEMAP grant award # G13AC000243 to the Wyoming State Geological Survey.

Mapping was conducted through on-the-ground examination and measurement of rock units, aerial imagery interpretation, and compilation of previous mapping and written reports. Initial mapping of the quadrangle began with aerial photographic interpretation by Wayne M. Sutherland and W. Dan Hausel during 2001 and 2002, which was incorporated into the 1:100,000 scale Rattlesnake Hills 30' x 60' quadrangle (Sutherland and Hausel, 2003). Initial Cenozoic interpretations were based on Love's (1970) 1:125,000 scale map and Van Houten's (1964) 1:62,500 scale map. Field work encompassed more than 28 days and over 100 miles walked by the authors between April and mid-July 2014. Earlier investigation was assisted by Robert W. Gregory in 2013. Photos are by Wayne M. Sutherland and Elizabeth C. Cola.

Although no economic rare earth or metals deposits were encountered, this investigation provided geologic details including more accurate radiometric dates for previously unmapped Paleoarchean-Mesoarchean rocks. This helps to better understand central Wyoming's Precambrian geology and structure, including the major shear and continental accretion zone referred to as the Oregon Trail structural belt. Mapping also clarified the relationships between Tertiary formations near the North Granite Mountains Fault.

We wish to acknowledge the Split Rock Ranch for access to their private lands to complete this map.

Location and Geologic Setting

The Mc Intosh Meadows 1:24,000 scale quadrangle in central Wyoming (fig. 1) is approximately 73 air km (45 mi) southeast of Riverton, and 26 km (16 mi) northeast of Jeffrey City. Elevations range from about 2,012 m (6,600 ft) above sea level in the southwestern corner of the quadrangle to over 2,225 m (7,300 ft) near the northern edge. The climate within the quadrangle is high desert; grasses and sage represent the majority of vegetation. Isolated pine and juniper trees are found at the higher elevations, with wetter environment vegetation growing along West Sage Hen Creek, Diamond Springs Draw, and their branches.

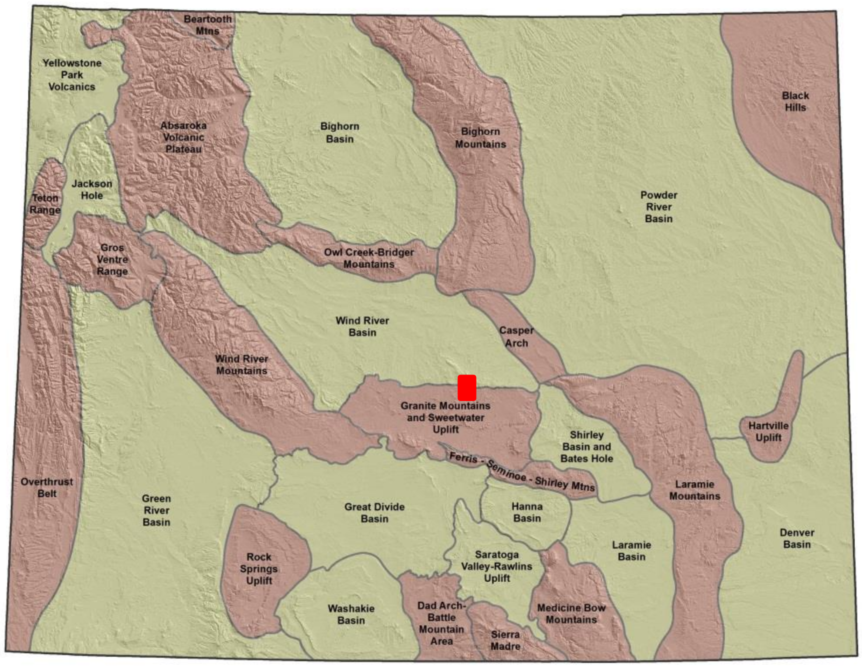

Figure 1. Approximate location of the Mc Intosh Meadows quadrangle

Access to the area is from the graded Agate Flat Road (BLM Road 2404), which leaves U.S. Highway 287 (Wyoming State Highway 789) about 10.5 km (6.5 mi) east of Jeffrey City and diagonals northeasterly across the southern half of the quadrangle, beginning about 21 km (13 mi) northeast of the highway. This road was known historically as the Waltman- Sweetwater Freight Road. Several side roads of varying conditions branch off Agate Flat Road providing general access to the remainder of the quadrangle.

The Mc Intosh Meadows 1:24,000-scale geologic map, is located in the Granite Mountains, within the ancient Precambrian craton known as the Wyoming Province (Condie, 1976; Houston, 1983). Geologic units within the quadrangle are either Quaternary, Tertiary, or Archean in age. Quaternary units are represented primarily by alluvium along drainages that include sand, gravel, and cobbles, along with slope wash and some minor landslides.

Tertiary rock unit exposures are dominated by the Miocene Split Rock Formation and the Eocene Wagon Bed Formation. The Oligocene White River Formation crops out north of the North Granite Mountains Fault system as a channel deposit. Eocene volcanic and subvolcanic rocks crop out four miles to the East, but are not known from within the quadrangle. No Paleozoic or Mesozoic units are known to crop out within the quadrangle. However, lower Cenozoic and Mesozoic units are inferred in subsurface of the A-A” cross section based on stratigraphic interpretation of a gamma ray log from the plugged and abandoned Atlantic Richfield Company Diamond Springs oil and gas well (49-013-06939) noted on the map.

The Archean rocks of the Granite Mountains were accreted onto the Wyoming Craton from approximately 2.65 to 2.63 Ga (Grace and others, 2006). They comprise a metamorphic complex of gneisses, schists, and fragments of supracrustal rocks that have been metamorphosed to amphibolite grade, intruded by medium to coarse grained granites, and subsequently intruded by diabase dikes

(Peterman and Hildreth, 1978). This metamorphic complex includes gneisses, pegmatites, granites, metapelites and quartzites of the Barlow Springs Formation, metagraywacke and metabasalt of the Rattlesnake Hills Group, and the Paleoarchean Sacawee and Antler orthogneisses.

The Granite Mountain batholith intruded the area around 2.62 Ga (Frost and others, 1998). East- to northeast-trending mafic dikes intruded during two intervals at approximately 2.4 to 2.6 Ga (Langstaff, 1995) and 1.47 to 1.45 Ga (Chamberlain and Frost, 1995; Chamberlain and others, 2000; 2003).

Structure

Numerous pervasive, dominantly ductile, east- to northeast-trending shear zones with steep southerly dips cut Archean rocks within the quadrangle. Due to their pervasiveness, only some of the larger, more concentrated shears are depicted on the map. The wide zone of shearing, related to the continental collision and accretion processes (Chamberlain and others, 2003; Frost and others, 2006; Grace and others, 2006), trends generally eastward across the entire central Granite Mountains and is referred to as the Oregon Trail structural belt.

Archean deformation was generally ductile. Conversely, Laramide deformation was typically brittle. The presence of both brittle and ductile deformation on some structures in the Granite Mountains indicates that some Archean structures were reactivated during the Laramide orogeny (Hausel, 1996). Ductile deformation is most prevalent at unit contacts as well as in gneissic layers of the Antler orthogneiss. Brittle faults and joints are easily observed in the East Sage Hen granite.

The Precambrian-cored Granite Mountains are a 137 km (85 mi) long by 48 km (30 mi) wide, west-trending, anticlinal uplift that developed during the Laramide Orogeny, beginning in latest Cretaceous time. The north flank of the uplift is gently sloping, whereas the south and west flanks are steeper and thrust-faulted. The 80 km (50 mi) long Emigrant Trail Thrust Fault, active during earliest Eocene time, marks this boundary. It slopes upward at 20 to 35 degrees to the south and west and has a throw of more than 4,570 m (15,000 ft) in some places. The western part of the thrust remained static after its movement, but extensive normal faulting modified the southern part of the thrust plate, particularly east of Crooks Gap near the end of early Eocene time (Love, 1970).

The North Granite Mountains Fault, as described by Love (1970), is one of the largest and most easily recognized structural features on aerial imagery within the Mc Intosh Meadows quadrangle. It generally separates the Wagon Bed Formation in the northern part of the quadrangle from the upper part of the Split Rock Formation to the south. However, the on-the-ground fault trace is mostly obscured by residuum from these two formations, with only a few definitive outcrops marking it. The trace of the fault hosts several springs, while earlier fluid movements along it are marked by areas of iron staining and the occurrence of dogtooth spar in some fractures. Many of the faults indicated on the quadrangle were determined by linear features seen from aerial imagery paired with slight changes in ground cover appearance.

The first phase of uplift in the area caused nearly a 2,250 m (7,500 ft) vertical increase of the Granite Mountains arch and subsidence of basins to the north and south. Uplift of the arch continued through the Paleocene and into the early Eocene. The compressional force causing the uplift also produced thrust faults, reverse faults, and subsidiary anticlines and folds. Near the end of the early Eocene (49-55 Ma), the Granite Mountains block, was uplifted as much as 1,500 m (5,000 ft) along the North Granite Mountains Fault System on their north side, and a greater amount along the South Granite Mountains Fault System on their south side. Both of these faults cross-cut preexisting structures and appear to be unaffected by rock types. By middle Eocene, Laramide orogenic compression had stopped which allowed preservation of the Wagon Bed formation.

During Miocene time, the 129 km (80 mi) long west-northwest-trending Split Rock syncline began to form along the Granite Mountains trend. This 48 km (30 mi) wide down-warp, with its axis several miles south of the Mc Intosh Meadows quadrangle, affected all earlier structures, subsided more than 915 m (3,000 ft), and is apparently still active (Love, 1970). Sedimentation into the syncline included the Miocene Split Rock Formation and the Pliocene Moonstone Formation. During Pliocene time, both the North and South Granite Mountains fault systems reactivated with a reversal of movements, dropping the Granite Mountains downward by as much as 305 m (1,000 ft) along the northern fault and 610 m (2,000 ft) along the southern fault (Love, 1970).

The Mc Intosh Meadows quadrangle, in its entirety, lies within the Oregon Trail structural belt, and the North Granite Mountains Fault system can be seen in an E-W trend cutting the northern third of the quadrangle. The majority of the West Sage Hen Rocks crop out in the southeastern corner of the quadrangle. They are included in the Sacawee Block, a narrow belt of Paleo- to Mesoarchean crust that extends in an east-west trend across the Granite Mountains. The West Sage Hen Rocks, near the southern boundary of the map, also contain numerous east-trending shear zones. Metamorphic zircon dates provided a date of shearing/deformation at about 2.65 Ga (Grace and others, 2006). The majority of Precambrian units within the Mc Intosh Meadows quadrangle exhibit deformational textures to varying degrees.

Economics

Abundant agates and small amounts of opal, rubies, and nephrite jade have been found within the Mc Intosh Meadows quadrangle. Occurrences in nearby areas indicated the potential for other mineral resources that include gold and associated metals, rare earth elements (REE), and uranium. However, no anomalous concentrations of these mineral resources were found while mapping the quadrangle. Recent exploration for both gold and REE by companies and individuals has focused on the Eocene volcanics and related alteration zones within Precambrian rocks east of the quadrangle. Recent drilling by one company indicated a potential for economic iron deposits 13 km (8 mi) east of the quadrangle.

The Wind River Formation in the Gas Hills, just north of the McIntosh Meadows quadrangle, contains significant concentrations of ore grade uranium deposits. The Gas Hills area has produced over 100 million pounds of U_3O_8 concentrate (yellowcake) since mining began in the 1950s. Although any uranium ore deposits within the map boundary lie at depths of a few hundred feet or more, historic prospect pits dot the northern part of the quadrangle, and numerous claims cover the northwestern part of the map. At least one company has explored an area to the west (in a similar geologic setting) and reports nearly a million pounds of indicated uranium resources. No current drilling information in that area is available to the public at this time (R.W. Gregory, personal communication, August 2014).

Agates of several types, including Sweetwater agates, are found within the Split Rock Formation across much of the quadrangle. During mapping, opal was discovered within a tuffaceous, sandy conglomerate in the upper porous sandstone sequence of the Split Rock Formation. Detrital nephrite jade has been reported from within the quadrangle, although none was found during the course of mapping. Similarly, rubies within gneiss and schist are known from the West Sage Hen Rocks in the southern part of the quadrangle. Rarely, quartz veins in the West Sage Hen Rocks yield euhedral, columnar, bipyramidal crystals. These crystals are vitreous with striations, vary from milky to clear and smoky, and are up to 7 cm (2.8 in) in length and 3 cm (1.2 in) in diameter.

Three oil exploration drill holes within the quadrangle were plugged and abandoned in 1958 or earlier (Wyoming Oil and Gas Conservation Commission website, 2014). A lack of exploration, coupled with complex structures, suggests that further oil and gas investigation may be warranted.

Samples

A total of 25 samples were collected, of which 16 were chosen for thin sections, 8 for geochemical analyses, 9 for x-ray diffraction, and 2 for radiometric dates. These samples are noted on the map as S1, S2, etc… Table 1 below gives a brief description and lists the analyses conducted per sample.

Table 1: McIntosh Meadow Samples

Map Symbol	Sample ID	Unit	Thin Section	Chemical Analysis	Radiometric Dating	X-ray Diffraction	Sample Description
S1	20140506LC-B	Agna	√				white-pinkish quartzite
S2	20140507WS-A	Agna	√			√	green quartzite
S3	20140507LC-A	Xd/Ad	√	√		√	altered ultramafic
S4	20140507LC-B	Xd/Ad	√			√	altered ultramafic/volcanic
S5	20140508WS-A	Agna	√	√		√	green micaceous quartzite
S6	20140508LC-A	Xd/Ad	√	√		√	altered ultramafic/volcanic
S7	20140508LC-B	Xd/Ad	√			√	sheared, altered ultramafic/volcanic
S8	20140520LC-A	Xd/Ad	√	√		√	radiating, acicular amphibolite, altered ultramafic/volcanic
S9	20150520LC-B	Agna	√	√	√		blue-grey quartzite, fibrous in part
S10	20140521LC- A	Abs	√			√	garnet-rich amphibolite
S11	20140521LC-C	Agna	√				felsite
S12	20140528WS-A	Agna	√			√	blue-grey quartzite
S13	20140528LC-A	Agna	√	√			coarse, granitic orthogneiss
S14	20140529WS-A	Argn	√	√			red banded gneiss and pegmatite
S15	20140530WS-A	Agna	√	√	√		plagioclase and biotite orthogneiss
S16	20140530WS-B	Xd/Ad	√				fine-grained, brown dike

Thin sections were prepared by Spectrum Petrographics of Vancouver, WA. Descriptions of thin sections are included in Appendix I and under Map Unit Descriptions where appropriate. Geochemical analyses, including whole rock chemistry, trace elements, rare earth elements, and gold were completed by ALS Chemex of Reno, Nevada. Geochemical analyses on samples included whole rock analyses (major element concentrations in the form of oxides) by inductively coupled plasma (ICP), atomic emission spectrometry or mass spectrometry, and atomic adsorption. X-ray diffraction and analysis was conducted at the Wyoming State Geologic Survey by Elizabeth Cola. Radiometric dating was conducted under the direction of Dr. Kevin Chamberlain, Department of Geology and Geophysics, University of Wyoming.

The samples collected for geochemical analyses are grab samples, which generally do not represent a large or measured volume of material greater than that of the sample itself. Elemental concentrations associated with a grab sample may or may not extend into the outcrop from which the sample was collected. Analyses of these samples can neither confirm nor deny the presence or absence of economic concentrations of various elements.

Prior to this mapping effort, several samples were collected and analyzed in conjunction with a state-wide survey of potential sources of rare earth elements (Sutherland and others, 2013). Sample results from both projects including descriptions, photographs, and analyses are available for examination in the Wyoming State Geological Survey's Wyoming Database of Geology (Wyo-DOG) at http://www.wsgs.uwyo.edu/Research/Minerals/Wyo-Dog.aspx. Whole rock analyses for samples collected within the Mc Intosh Meadows quadrangle during this project are shown in tables 2 and 3.

Table 2: Bulk Geochemistry

Sample ID:	S3	S5	S6	S8	S9	S13	S14	S15
SiO_2 (%)	46	71.8	62.5	77.1	72.2	35.8	70.5	74.9
Al_2O_3 (%)	7.1	13.5	16.85	11.45	14.45	33.9	12.15	13.8
TiO_2(%)	0.34	0.26	1.25	0.28	0.23	0.29	0.34	0.14
Fe_2O_3(%)	11.1	3.2	7.17	2.34	3.43	3.9	3.74	1.96
MnO(%)	0.16	0.03	0.08	0.02	0.04	0.06	0.05	0.03
MgO(%)	23.7	5.89	8.98	0.8	5.1	17.5	2.15	0.31
CaO(%)	4.35	0.09	0.75	0.18	0.04	0.08	0.18	1.97
Na_2O(%)	0.43	0.2	0.53	3.12	0.5	0.29	2.84	3.59
K_2O(%)	0.11	2.46	0.23	4.67	1.92	1.36	4.08	3.28
P_2O_5(%)	0.12	0.05	0.4	0.08	0.05	0.06	0.07	0.08
SrO(%)	<0.01	<0.01	<0.01	<0.01	<0.01	<0.01	0.01	0.03
BaO(%)	0.01	0.09	<0.01	0.15	0.05	0.03	0.05	0.14
C(%)	0.06	0.05	0.07	0.04	0.06	0.13	0.02	0.02
S(%)	0.03	0.02	0.01	<0.01	0.01	0.02	<0.01	<0.01
Total (%)	93.51	97.64	98.82	100.23	98.08	93.42	96.18	100.25

Table 3: Trace Element and Rare Earth Element Composition

Sample ID:	S3	S5	S6	S8	S9	S13	S14	S15
Ba (ppm)	89	789	38.4	1360	453	266	484	1175
Ce (ppm)	14.5	46.8	114	23.5	76.5	73.7	124	84.1
Cr (ppm)	2610	20	30	20	30	20	40	20
Cs (ppm)	0.08	0.5	0.43	0.24	0.71	1.16	0.48	0.27
Dy (ppm)	1.67	0.96	5.94	1.34	1	1.88	5.84	1.43
Er (ppm)	1.05	0.45	2.99	0.87	0.44	1.3	4.13	0.62
Eu (ppm)	0.39	0.51	2.11	0.39	0.57	0.64	0.39	1.01
Ga (ppm)	9.1	16.5	23.8	9.7	18.8	38.1	14.2	15.8
Gd (ppm)	1.63	1.47	6.58	1.18	1.81	1.87	4.74	2.48
Hf (ppm)	1	4.2	6.4	5.2	5.6	5.3	7.2	4.2
Ho (ppm)	0.34	0.19	1.2	0.32	0.16	0.42	1.36	0.27
La (ppm)	7.4	28.2	61.1	12.6	49.5	44	62.6	48.1
Lu (ppm)	0.14	0.06	0.42	0.12	0.08	0.22	0.76	0.1
Nb (ppm)	1.8	2.5	12.9	5.7	4.8	6.1	31.7	4.6
Nd (ppm)	6.1	14.3	44.9	7.5	21.6	24.8	36.2	28.6
Pr (ppm)	1.7	4.44	12.2	2.31	6.96	7.46	11.7	8.65
Rb (ppm)	2	60.8	8	77.1	69.2	39.2	164.5	67.1
Sm (ppm)	1.48	2.09	8.12	1.35	2.97	3.52	6.13	4.2
Sn (ppm)	1	1	3	1	2	1	8	1
Sr (ppm)	15.6	10.7	17.7	42.4	6.7	8.2	42.9	208
Ta (ppm)	0.1	0.2	0.8	0.5	0.3	0.6	3.8	0.3
Tb (ppm)	0.28	0.19	1.09	0.22	0.22	0.27	0.9	0.31
Th (ppm)	2.25	8.99	9.54	4.38	14.3	8.59	65.7	11.25
Tm (ppm)	0.16	0.07	0.45	0.14	0.04	0.21	0.7	0.1
U (ppm)	0.72	0.91	1.24	0.66	1.13	1.22	4.42	1.14
V (ppm)	115	18	128	17	23	60	76	45
W (ppm)	1	2	5	1	6	1	5	4
Y (ppm)	9.1	5	31.7	7.8	5.5	12.7	39.2	6.8
Yb (ppm)	1.02	0.41	2.84	0.87	0.39	1.46	4.85	0.51
Zr (ppm)	34	163	269	216	230	194	239	154
As (ppm)	6.5	0.5	0.2	0.8	1	1.2	5.5	1.5
Bi (ppm)	0.04	0.01	0.01	0.02	<0.01	0.01	0.03	<0.01
Hg (ppm)	0.044	0.005	<0.005	<0.005	0.01	<0.005	<0.005	<0.005
Sb (ppm)	0.13	0.05	<0.05	0.09	<0.05	<0.05	0.07	<0.05
Se (ppm)	<0.2	<0.2	0.6	0.2	0.2	<0.2	0.9	0.2
Te (ppm)	0.01	<0.01	<0.01	<0.01	<0.01	<0.01	0.01	<0.01
Tl (ppm)	<0.02	0.03	0.02	0.04	0.16	0.18	0.04	0.11
LOI (%)	5.4	4.16	1.91	1.22	3.89	7.19	1.96	0.73
Total* (%)	99.18	101.73	100.65	101.41	101.9	100.46	98.13	100.96

*Total includes oxides in Table 3

Ag (ppm)	<0.5	<0.5	<0.5	<0.5	<0.5	<0.5	<0.5	<0.5
Cd (ppm)	<0.5	<0.5	<0.5	<0.5	<0.5	<0.5	<0.5	<0.5
Co (ppm)	76	6	17	6	6	11	4	3
Cu (ppm)	9	1	<1	5	2	1	3	16
Li (ppm)	<10	10	40	<10	20	30	10	<10
Mo (ppm)	<1	<1	<1	1	1	1	1	<1
Ni (ppm)	1070	7	16	5	3	59	13	3
Pb (ppm)	3	<2	<2	9	<2	<2	15	22
Sc (ppm)	15	2	14	2	1	2	9	1
Zn (ppm)	132	24	163	9	51	53	36	28

Several analyses are of interest from the geological as well as the possible economic perspective. Geologically, the bulk chemistry validates the type of rock at each locality. For example, S5 and S9 confirm the identification of quartzite and S8, S14, and S15 confirm the identification of a felsic igneous rock. The rocks identified in the field as altered ultramafics were categorized geochemically as peridotite (S3), gabbro (S6), and amphibolite (S13). Economically, there could be potential interest in mafic-ultramafic samples with elevated chromium and nickel such as sample S3. Many of the altered rocks have undergone metasomatic alteration. The influx of hot fluid during this alteration has the potential to change the presence of trace elements and REEs in the rocks bringing them into an economical range.

Description of Map Units

Quaternary

Alluvium (Qal): Alluvium comprises unconsolidated clay, silt, sand, and occasionally coarse gravels and cobbles located in and along most drainages within the quadrangle. This unit was mapped using both aerial imagery interpretation and field observations. It may include some eluvial deposits, slope wash, and small alluvial and colluvial fans along drainages.

Tertiary

Miocene *Split Rock Formation:* The upper part of the Miocene Split Rock Formation crops out over the largest area of any geologic formation within the Mc Intosh Meadows 7.5' quadrangle and dominates the southern two thirds of the quadrangle. Typically, it is near flat-lying, with most dip angles less than ten degrees southward into the Split Rock syncline. Extensive cross-bedding often obscures measurement of its apparent overall south to southeasterly dip. The Split Rock Formation lies unconformably on top of the Eocene Wagon Bed Formation (Van Houten, 1964; Love, 1970) and the Oligocene White River Formation. The Split Rock Formation also locally laps directly onto Precambrian rocks.

Lithologically, the Split Rock Formation as described by Love (1961) is a massive, well-sorted, yellowish-gray to grayish-orange, volcanic sandstone with persistent beds of coarse conglomerate. The conglomerate beds are composed of angular to rounded pebbles and cobbles derived from the Rattlesnake Hills volcanics and from Precambrian units. Much of the finer volcanic material within the formation is suggested to have the Yellowstone-Absaroka area as a source (Van Houten, 1964; Love, 1970). The Split Rock Formation sandstones differ from all other Tertiary age sandstones in the vicinity in that they contain conspicuous well-rounded and frosted grains (Love, 1970). Irregular chert nodules and siliceous aggregates can be found throughout the formation.

Regionally, the Split Rock Formation ranges in thickness from 46 m (150 ft) to more than 305 m (1000 ft); however, its thickness within the Mc Intosh Meadows quadrangle has not been measured. Love (1970) divided the formation into four identifiable units from bottom to top: a lower porous sandstone sequence, a clayey sandstone sequence, a silty sandstone sequence, and an upper porous sandstone sequence. The upper and lower porous sandstone sequences comprise most of the Split Rock outcrop within the Mc Intosh Meadows quadrangle. However, the silty sandstone sequence was exposed in one small outcrop along East Diamond Springs Creek in the SW¼SE¼NE¼, Sec. 35, T32N, R90W. Unit thicknesses are variable, and from bottom to top respectively are: lower - up to 152 m (500 ft); clayey - 30–91 m (100–300 ft); silty - 91–183 m (300–600 ft); and upper - up to 305 m (1,000 ft).

Rachou (1951) found early middle Miocene mammal fossils in the upper part of the Split Rock Formation about 19 km (12 mi) east of the Mc Intosh Meadows quadrangle. These were found northeast of Dry Creek and south of the North Granite Mountains Fault in Love's (1970) silty sandstone sequence. However, no fossils were found during field investigations for this map.

Upper porous sandstone sequence (Tsru): The upper porous sandstone sequence is dominated by medium- to coarse-grained, gray to buff, massive to coarsely cross-bedded sandstone with abundant rounded, frosted, and clear quartz grains, red hematite-stained grains, and brilliant, clear, slightly abraided quartz bipyramids. This is accompanied by abundant (0.36 to 5.1 percent of the sandstone) tiny (0.1 mm; 0.04 in) black subrounded magnetite grains. Pure bluish-white pumicite beds as much as 3 m (10 ft) thick, with curved or rectilinear, pink to colorless shards are included within this upper sequence (Love, 1970).

Within the Mc Intosh Meadows quadrangle, the top of the upper porous sandstone sequence is represented by resistant coarse-grained, cross-bedded conglomerate (fig. 2) that persistently caps hills and buttes; poorly cemented or weathered exposures often appear similar to Quaternary terrace deposits. The conglomerate is variable in thickness, up to 15 m (50 ft), and in some areas splits into multiple layers separated by fine-grained sandstone and ash beds. The conglomerate is underlain by white to cream and tan, very fine- to fine-grained, tuffaceous sandstone and ash layers. Scattered Sweetwater agates are often found in the residuum of the upper porous sandstone sequence and help to distinguish between adjacent outcrops of similar lithologies in the Split Rock Formation and those in the Wagon Bed Formation where the agates are absent.

Figure 2. Upper Split Rock conglomerate layers

Sweetwater moss agates (fig. 3; as described by Endlich, 1879, p.113) are found across much of the quadrangle in a conglomerate and sandstone layer in the bottom 30 m (100 ft) of the upper porous sandstone sequence. These are subrounded, frosted, translucent gray to red and brown and contain black manganese dendrites. The agates are commonly less than 2.5 cm (1 in) in diameter, moderately radioactive, and many fluoresce brilliant yellow. Love (1970) speculated that these may have been derived from the reworking of agates from the lower porous sandstone sequence.


Figure 3. Assorted Sweetwater Agates

Silty sandstone sequence (Tsrs): The silty sandstone sequence appears as a buff to white, fine-grained sandstone interbedded with tuff and pumicite. A silty matrix within the sandstone is common throughout this unit, as is the presence of abundant glass shards (Love, 1970). As mentioned earlier, this sequence was identified in only one location in Sec. 35, T32N, R90W. Both the silty sandstone sequence (Tsrs) and the clayey sandstone sequence (Tsrc) are included in the subsurface interpretation of cross sections A-A" and B-B".

Clayey sandstone sequence (Tsrc): The clayey sandstone sequence is composed almost entirely of a gray, fine- to medium- grained, very soft, clayey sandstone. Glass shards are numerous throughout this unit (Love, 1970). This sequence was not observed in the quadrangle.

Lower porous sandstone sequence (Tsrl): Love's (1970) lower porous sandstone sequence has a 15 to 30 m (50- to 100 ft) thick pebble and cobble conglomerate within a mudstone matrix as a base which lies unconformably on the White River Formation. Above this conglomerate is a thick deposit of well-rounded, well-sorted volcanic sandstone with local beds of gray vitric tuff and lenses of conglomerate. This sandstone containing tuff beds is characteristic of the Split Rock Formation throughout the Sweetwater plateau (Van Houten, 1964). The vitric tuff is often pure enough for use as abrasive pumicite (Love, 1970). Sweetwater-type agates, 2.5 to 10 cm (1 to 4 in) in diameter, are found in a hard, gray, arkosic conglomeratic sandstone 91 to 122 m (300 to 400 ft) above the base of this sequence and may be the source of the smaller, more rounded agates found in the upperporous sandstone sequence (Love, 1970). Poorly cemented or weathered conglomerate exposures in the lower porous sandstone sequence that cap ridges often appear similar to Quaternary terrace deposits.

Oligocene *White River Formation (Twr):* The White River Formation overlies the irregular surface of the Wagon Bed Formation and commonly cuts into the Wagon Bed as channel deposits 76m (250ft) deep or more (Van Houten, 1964). The base of the White River is an arkosic, gray sandstone and conglomerate that grades upward into massive white to grayish-orange, cliff forming, fine-grained, silty sandstone and blocky hard siltstone and claystone that form the bulk of the formation in the western Beaver Divide area. Thin beds of white tuff occur in some localities. Within the quadrangle, the White River occurs north of the North Granite Mountains Fault and appears to be a channel (fig. 4) within the Wagon Bed Formation. The lower porous sandstone sequence of the Split Rock Formation caps the White River with a poorly exposed contact, often recognized by a subtle erosional bench on slopes. Minor springs also mark this contact between the White River and the overlying Split Rock in some areas.

Figure 4. Contact between the white-tan White River Fm. (right) and the orange-tan Wagon Bed Fm. (left) shows a channel cut into the Wagon Bed Fm. that was filled with the White River Fm.

Middle–late Eocene *Wagon Bed Formation (Twb):* The Wagon Bed Formation is stratigraphically equivalent to the Bridger Formation in the Green River and Great Divide Basins (Love and others, 1993). Regionally, the Wagon Bed varies from pale-olive and greenish-gray tuffaceous sandstone, siltstone, and mudstone, with some ash layers to a highly variable coarse conglomerate. The thickness of the Wagon Bed as measured by Van Houten (1964) ranges from about 40 m (130 ft) to more than 213 m (700 ft), and may be on the order of about 183 m (600 ft) near the Rattlesnake Hills volcanic centers a few miles east of the Mc Intosh Meadows quadrangle (Love, 1970).

The lower half of the formation as described by Van Houten (1964) in the Beaver Rim area, about 55 km (34 mi) west of the Mc Intosh Meadows quadrangle, contains abundant pyroclastic debris along with pebbles and cobbles of sodic trachyte, with the upper half dominated by coarse detrital alkalic andesite material ranging in size from pebbles to boulders. The upper part of the formation is poorly-sorted, whereas the remainder is generally composed of well-sorted beds of yellowish-green to pale olive and dark greenish-gray sandstone, siltstone, and mudstone. Persistent ledge-forming mudstones mark the base of the formation. Ash, derived both locally and from the Yellowstone-Absaroka area, forms thick deposits exhibiting no bedding or sorting in the middle part of the formation. The middle and upper parts of the formation also contain light to pale yellowish-gray, coarse-grained lapilli tuff, biotitic vitric tuff, and tuffaceous sandstone. Composition of volcanic materials within the Wagon Bed suggests that latitic eruptions, found dominantly in the eastern and western Rattlesnake Hills, are older than the phonolitic and trachytitic eruptions found dominantly in the central Rattlesnake Hills (Van Houten, 1955).

Locally, the middle and upper Wagon Bed Formation crops out in the northern part of the Mc Intosh Meadows quadrangle, where it is dominated by coarse, cross-bedded conglomerates, sandstones, and ash layers. Conglomerate clasts vary from dominantly Precambrian debris to dominantly local volcanic materials. Clasts range from angular to rounded with sizes ranging up to 30 cm (12 in) at some localities. The matrix varies from gray to tan to limonite-stained and rusty red, fine- to coarse-grained arkosic sandstone, to cream silt, clay, and white ash. The conglomerate is poorly cemented in some areas but silicified in others.

Radiometric ages (K-Ar) from samples collected and analyzed by Evernden and others (1964) date a bentonitic tuff in the lower Wagon Bed Formation at 49.0 Ma in the Green Cove area along Beaver Rim about 55 km (34 mi) west of the Mc Intosh Meadows quadrangle. In the same area, at Wagon Bed Spring, they calculated an age of 45.4 Ma for a biotitic tuff near the middle of the Wagon Bed Formation. They derived a similar age of 45.0 Ma for an andesitic tuff in the Wagon Bed (Tepee Trail) Formation near Badwater, about 72 km (45 mi) north of the quadrangle. Black (1969) reported a Wagon Bed age, also from the Badwater area, of 42.3 ± 1.4 Ma.

Precambrian

Proterozoic and Neoarchean *mafic dikes (Xd/Ad):* Diabase, amphibolite, and related mafic dikes of two ages occur within the Mc Intosh Meadows quadrangle. Older Archean dikes (ca. 2.68 Ga; Grace and others, 2006) tend to be boudinaged and discontinuous as compared to similarly oriented younger dikes dated at 2.115 Ga (K.R. Chamberlain personal communication, September 2014) that are near vertical, relatively straight, uniform in thicknesses, predominately trend east-northeast, and cross-cut most other Precambrian units and structures (Chamberlain and others, 2000). Langstaff (1995) noted that epidote-quartz alteration between 2.4 and 2.6 Ga (after Ludwig and Stuckless, 1978; and Peterman and Hildreth, 1978) locally affects some of the dikes. Grace and others (2006) noted a 2649 ± 2.8 Ma shearing event in a 2m (6.5 ft) thick amphibolite dike in the West Sage Hen Rocks in the southern part of the quadrangle.

The older dikes (fig. 5) often contain cordierite and olivine grains replaced by serpentine and various metamorphic amphiboles such as hornblende, actinolite, tremolite, and gedrite. The interpretations of these minerals and textures suggest the source of these rocks is ultramafic or volcanic. Metavolcanics are known in the vicinity and the area is part of a known continental collision zone; thus, either origin is a possibility. However, it is difficult to determine the exact origin based on the lack of outcrop and extreme metamorphism that has overprinted the rock. Based on the presence and type of hydrated minerals, it is most likely the rock underwent extensive metasomatism pre- and/or syn- metamorphism and was exposed to post-metamorphism hydrothermal alteration.

Figure 5. Altered ultramafic or volcanic, older Archean dike

Red gneiss (Argn): A red, granitic orthogneiss and pegmatite, unlike the other Precambrian units, is constrained in outcrop by only one contact with the Sacawee Orthogneiss. The age and origin of this gneiss are unknown, but the age is suspected to be Archean. The outcrop is easily visible from aerial photography as a rusty area. The rock is dark pink to red, medium to course grained, and typically contains a chlorite foliation.

Neoarchean *Quartz/pegmatite veins and dikes:* Quartz/pegmatite veins and dikes are abundant, but have not been mapped as a separate unit due to the generally small size of their outcrops. Quartz/pegmatite veins and dikes vary upward in width from less than 2.5 cm (1 in) to irregular areas more than 10 m (33 ft) across. These are dominated either by quartz or feldspar, but contain both. The pegmatites either cross-cut or run parallel to foliation, layering, and structure throughout the area, and may or may not be sheared. Two or more generations of pegmatite are found within the quadrangle; the earlier pegmatites are sheared or foliated while more extensive pegmatites appear to be unsheared and unfoliated and are therefore probably younger.

Neoarchean *shear zones (SZ):* Numerous shear zones cut most Archean rocks within the Mc Intosh Meadows quadrangle with variable degrees of shearing. Areas indicated on the map are locations of extreme shearing. Typically, sheared rock appears in easily weathered vertical layers. Shearing is so strong it is sometimes difficult to distinguish the original rock type. Examples of these shear zones in the Antler orthogneiss show very sheared orthogneiss with more resistant quartzite layers.

Shearing of an amphibolite dike, about 2m thick that cuts the Sacawee orthogneiss in the West Sage Hen Rocks in the southern part of the quadrangle, is dated at 2649 ± 2.8 Ma by Grace and others (2006). This shearing age is synchronous with the timing of deformation for the northwest-trending McDougal Gulch shear zone several miles northeast of the quadrangle, which juxtaposes McDougal Gulch metavolcanics of the Rattlesnake Hills Group upon the older Barlow Gap Group. The McDougal Gulch deformation is directly dated at 2,645 ± 6 Ma based on U-Pb titanite data from mylonitized metabasalt (Frost and others, 2006).

Neoarchean *East Sage Hen granite (Ash):* The East Sage Hen granite is a pink- to orange-weathering, medium- to coarse-grained, unfoliated to weakly foliated, biotite granite dated by Langstaff (1995) to have a minimum crystallization U/Pb age of 2,622 ± Ma, although a maximum is projected at 2,650 Ma. The granite contains abundant quartz, microcline, and oligoclase, along with about two percent biotite. Langstaff (1995) noted accessory minerals to include hornblende, epidote, sphene, allanite, apatite, and zircon. He also reported xenoliths of the Barlow Springs Formation, the Sacawee orthogneiss, and other pre-existing rock units within the East Sage Hen granite. The granite is extensively sheared where it crops out in the southeastern part of the quadrangle near the east end of West Sage Hen Rocks. Strong shearing is also present along the entirety of its contact with the Antler Orthogneiss.

Rattlesnake Hills Group

Mesoarchean *McDougal Gulch Metavolcanics (Amb):* The McDougal Gulch Metavolcanics are dominated by amphibolite gneisses representative of metabasalts. Only one poorly exposed outcrop that is interpreted to be the McDougal Gulch metabasalts occurs near the east-central edge of the Mc Intosh Meadows quadrangle. Hausel (1996) described significant variability in the metabasalts and accompanying ultramafic schists within the formation about 16 km (10 mi) northeast of the Mc Intosh Meadows quadrangle. Hausel also noted that the foliation and apparent bedding of this formation are conformable with both the overlying UT Creek Formation and with the underlying Barlow Springs Formation. However, Langstaff (1995) states that the McDougal Gulch-Barlow Springs contact may have been obscured by deformation to the extent that contact relations may not be reliably interpreted.

Barlow Gap Group

Paleoarchean–Mesoarchean *Barlow Springs Formation (Abs):* The Barlow Springs Formation is interpreted as the base of the supracrustal units on top of meta-igneous rocks within the Granite Mountains-Rattlesnake Hills area (Bickford, 1977; Langstaff, 1995; Hausel 1996; Sutherland and Hausel, 2005). Quartzite, metapelite, banded iron formation, metafelsite, and amphibolite gneiss, intruded in places by metagabbro, are the main components of the formation. The amphibolite gneisses are both ortho-amphibolites (Hausel, 1996) and para-amphibolites, and include metabasalt, tremolite-chlorite schist, and anthophyllite gneiss (Bickford, 1977). Further detailed descriptions are found in Fruchey (2002) and Kruckenberg and others (2001). The Barlow Springs Formation is reported by Hausel (1996) to be primarily metasedimentary and lithologically similar to the Goldman Meadows Formation in the South Pass greenstone belt (Hausel, 1991), the Seminoe Formation in the Seminoe Mountains greenstone belt (Hausel, 1994), and Metamorphic Unit 2 in the Copper Mountain supracrustal belt (Hausel and others, 1985). The Barlow Springs Formation generally crops out along the southeast edge of the West Sage Hen rocks as well as in thin lenses surrounded by either the Antler orthogneiss or the Sacawee orthogneiss.

The base of the Barlow Springs Formation is a red to gray or fuchsitic green, massive to layered quartzite resting on top of older gneisses. Overlying the basal quartzite is a discontinuous, contorted, rusty- to greenish-brown, micaceous, quartzose schist up to 4.6 m (15 ft) thick (Sutherland and Worman, 2013). Similar thin quartzites and schists occupy more than one stratigraphic horizon within the Barlow Springs Formation. Thin layers and occasional large clusters of sillimanite crystals are hosted by these schists, particularly in areas that have been tightly folded. Several discontinuous layers and isolated lenses of banded, rusty-brown to black-weathered iron formation up to 21 m (70 ft) thick overlie the quartzose schist (Bickford, 1977). The presence of iron formation exposures within the Mc Intosh Meadows quadrangle is minimal.

Amphibolite gneiss interbedded with grey, micaceous quartzite overlies the banded iron formation. The amphibolite gneiss has been interpreted to be dominantly metabasalt (Langstaff, 1995), although it may include minor metagreywacke. Locally, this gneiss may grade laterally from black to bleached gneiss, to unlayered and unstructured massive bleached gneiss, and then into coarse-grained granite Bickford (1977). Pods and layers of metafelsite are found within the Barlow Springs and are most abundant near the upper part of the formation. These are often epidotized and may be gradationally interbedded with amphibolite or other rock types.

The Barlow Springs Formation lies on top of the Sacawee and older gneisses (Bickford, 1977; Hausel, 1996; Sutherland and Hausel, 2005). Deformation obscures many of these contacts and includes shearing of the gneiss, occasional shearing in the quartzite, some areas of in-folding extending over several feet, and minor areas exhibiting angular relationships between bedding in the quartzite and foliation in the gneiss. In a few limited outcrops, the Barlow Springs Formation appears to be conformable on top of the Antler orthogneiss.

Langstaff (1995) reported ages from detrital zircons in quartzite within the Barlow Springs Formation clustering at 3,300 Ma. He also reported a zircon age for metadacite in the upper part of the formation at 2,856 ± 55 Ma in an area about 16 km (10 mi) east of the Mc Intosh Meadows quadrangle and north of the North Granite Mountains Fault. Fruchey (2002) determined an essentially identical magmatic age of 2,864 ± 7.8 Ma for a similar metadacite from the upper part of the Barlow Springs Formation about 10 km (6 mi) to the east in the Blackjack Ranch quadrangle.

Field investigation there showed that Fruchey's location is within a severely sheared amphibolite gneiss cut by small quartz veins, and may be within the lower part of the overlying McDougal Gulch Metavolcanics rather than within the Barlow Springs Formation (Sutherland and Worman, 2013).

Basement Gneiss Complex

Paleoarchean *Sacawee orthogneiss (Agns):* The Sacawee is a distinctive coarse to medium grained, pink to tan, granitic-appearing, porphyritic gneiss (fig. 6) with generally strong foliation characterized by large potassium feldspar crystals. Bickford (1977) described the foliation as being defined by parallelism of biotite plates and is best observed where biotite is abundant. He also noted that locally, elongate tabular porphyroblasts of microcline, or blocky crystals of pink and blue perthitic feldspar paralleled regional lineation. Biotite is common and forms small mats and occasionally large enclaves as much as 30 m (100 ft) long and 1 m (3 ft) or more thick. Quartz stringers are also common, as are local gradations from coarse to medium to fine layers that maintain a similar overall appearance to the coarse-grained sections.


Figure 6. Deformed Sacawee orthogneiss

Langstaff (1995) noted that the Sacawee cuts older gneisses, such as the Antler, and contains xenoliths of the older gneisses in some areas. He also described large xenoliths of the Barlow Springs Formation within his older orthogneiss complex that includes the Sacawee. Field work east of this quadrangle and in adjacent areas indicates that some blocks of the Barlow Springs within the Sacawee are in-foldings rather than xenoliths. In the Mc Intosh Meadows quadrangle, the typical contact between the Sacawee and Antler is interfingered and sheared. It is common near the contact to see slivers of Sacawee within the Antler and vice versa. Fruchey (2002) calculated the age of the Sacawee to be 3,258 ± 8 Ma from a sample collected near Barlow Gap, 0.4 km (0.25 mi) east of the southeast edge of the quadrangle.

Paleoarchean *Antler orthogneiss (Agna):* The Antler orthogneiss is described by Fruchey (2002) as lenticular bodies of gray, fine-grained, finely layered, equigranular gneiss with foliation defined by alignment of biotite. The Antler orthogneiss has a wider variety of descriptions within the Mc Intosh Meadows quadrangle. The more "classic" description is a fine-grained, gray to pink, mylonized rock (fig. 7). There is also a gneissic feldspar-rich member which could be a less deformed version of the mylonite. Many lightly foliated quartzites are also present, ranging in coloration from blue-gray, dark gray, whitish-tan, to pink. In some locations, the blue-gray quartzite closely resembles the Mesoarchean Frank feldspathic metaquartzite mapped in the Stampede Meadows quadrangle (J.F. McLaughlin, personal communication, September 2014).

Fruchey (2002) described the relationships between the Antler and the Sacawee as ambiguous. Mapping within the quadrangle showed contacts between the Antler and the Sacawee to be variable. Contacts are commonly interfingered and sheared where lenticular areas of coarse-grained gneiss similar to the Sacawee appear to have intruded the Antler. In some areas, the contact is gradational with the biotite foliation in the Antler becoming stronger and darker toward its contact with the Sacawee. The Antler is also occasionally adjacent to the overlying Barlow Springs Formation, which may have been deposited directly on top of the Antler. However, the contact is often obscured due to shearing. Shear zones are common within the Antler, as they are throughout the Precambrian. As described earlier, these zones show intensely sheared vertical to sub-vertical layers, and the rock type is not always obvious. Typically, the most sheared rock appears to be orthogneiss with less shearing in the more resistant quartzite layers.

Figure 7. Mylonitic Antler orthogneiss

Langstaff (1995) dated the Antler at 3,370 ± 12 Ma from an outcrop east of the Mc Intosh Meadows quadrangle and referred to it as the "older orthogneiss", which he interpreted to have been intruded by the Sacawee.

Sample 20140530WS-A, representative of a fine-grained section of the Antler (fig. 8) in the southeastern part of the quadrangle, was processed for U-Pb dating (CA-TIMS) by Kevin R. Chamberlain (unpublished, 2014a) of the University of Wyoming Department of Geology and Geophysics. Eight single grain analyses produced concordant or nearly concordant data that do not overlap within error (Appendix II: Fig. 3, Table 1).

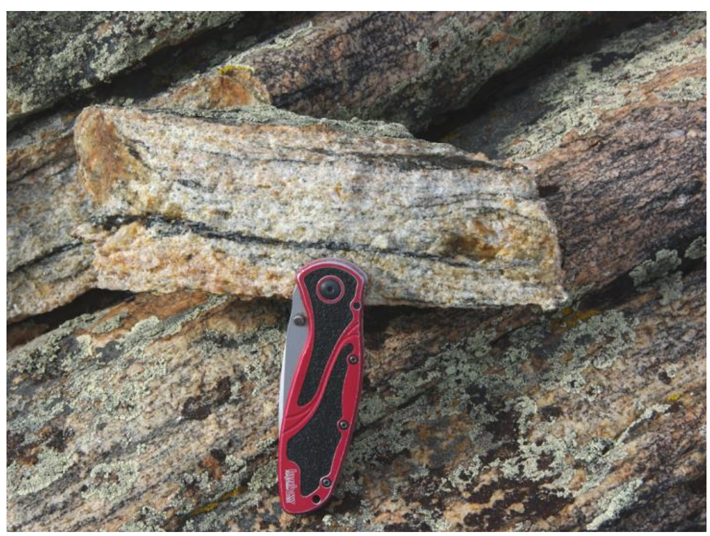

Figure 8. Sample 20140530WS-A, fine-grained, finely layered, Antler gneiss.

$^{207}Pb/^{206}Pb$ dates range from ca. 3,320 to 3,380 Ma (Appendix II: Fig. 4). Th/U values from all single grain analyses are similar and are consistent with magmatic growth. Data are interpreted to reflect magmatism ca. 3,325 Ma or younger, with inherited components as old as 3,372 Ma.

A second sample (20140520LC-B) of a bluish-black quartzite (fig. 9) within the Antler orthogneiss was also dated under the direction of Dr. Chamberlain (unpublished, 2014b). From this sample, a representative population of detrital zircons was analyzed by Laser Ablation Inductively Coupled Plasma Multicollector Mass Spectrometry (LA-ICP-MC-MS) at the University of California at Santa Barbara. Age distribution is heavily concentrated ca. 3.3 Ga, which is the age of the basal Sacawee and related gneisses; lesser peaks noted at ca. 3.1 Ga and 2.90 Ga are interpreted to represent the ages of other intrusions in the Barlow Gap area (Grace et al., 2006). Data in support of these conclusions and the report by Dr. Chamberlain are found in Appendix III.

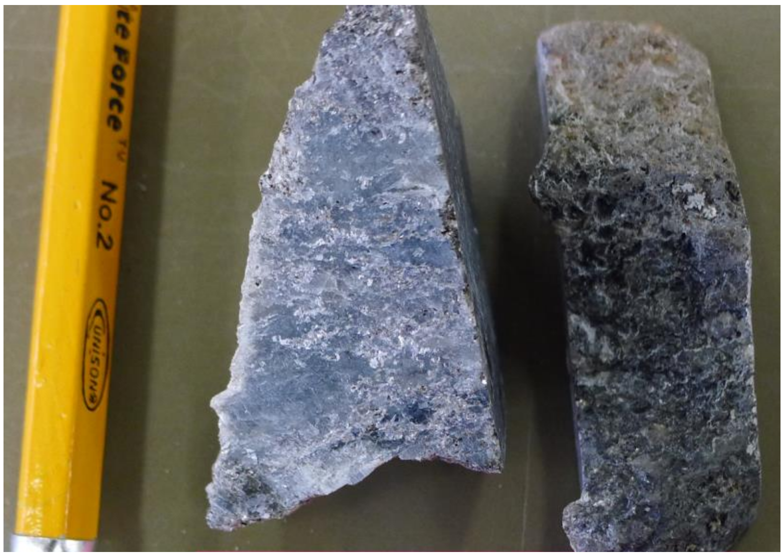

Figure 9. Sample 20140520LC-B, blue grey Antler quartzite

The Antler is interpreted to reflect periods of magmatism interspersed by periods of erosion and the deposition of sediments that were subsequently metamorphosed to quartzite.

References

* = Not cited in text

Bickford, F.E., 1977, Petrology and structure of the Barlow Gap area, Wyoming: Laramie, University of Wyoming, M.S. thesis, 76 p., scale 1:24,000.

Black, C.C., 1969, Fossil vertebrates from the late Eocene and Oligocene Badwater Creek area, Wyoming, and some regional correlations: Wyoming Geological Association Guidebook, 21st Annual Field Conference, p. 43-48.

Chamberlain, K.R., 2014a, Report on U-Pb date of the Antler Granite, Granite Mountains, Wyoming: unpublished, 7 p., 1 table.

Chamberlain, K.R., 2014b, Report on LA-ICP-MS dating of detrital zircons from 2014-05-20 LC-B: unpublished, 5 p., 2 spreadsheets.

Chamberlain, K.R., and Frost, B.R., 1995, Mid-Proterozoic mafic dikes in the central Wyoming Province: evidence for Belt-age extension and supercontinent breakup: Geological Association of Canada – Mineralogical Association of Canada annual conference, Abstracts, v. 20, p. A-15.

Chamberlain, K.R., Sears, J.W., Frost, B.R., and Doughty, P.T., 2000, Ages of Belt Supergroup deposition and intrusion of mafic dikes in the central Wyoming Province: evidence for extension at ca. 1.5 Ga and 1.37 Ga and potential piercing points for Rodinia reconstructions: Geological Society of America, Abstracts with Programs, v. 32, no. 7, p. A-319.

Chamberlain, K.R., Frost, C.D., and Frost, B.R., 2003, Early Archean to Mesoproterozoic evolution of the Wyoming Province – Archean origins to modern lithospheric architecture: Canadian Journal of Earth Sciences, v. 40, no. 10, p. 1357-1374.

Condie, K.C., 1976, The Wyoming Province of the western United States, in Windley, B.F., ed., The early history of the earth: John Wiley and Sons, New York, N.Y., p. 499-510.

Endlich, F.M., 1879, Report on the geology of the Sweetwater district, in Hayden, F.V., Eleventh annual report of the United States Geological and Geographical Survey of the Territories embracing Idaho and Wyoming, being a report of exploration for the year 1877: Washington, U.S. Govt. Printing Office, p. 3-158.

Evernden, J.F., Savage, D.E., Curtis, G.H., and James, G.T., 1964, Potassium-Argon dates and the Cenozoic mammalian chronology of North America: American Journal of Science, v. 262, p. 145-198.

*Fischer, L.B., and Stacey, J.S., 1986, Uranium-lead zircon ages and common lead measurements for the Archean gneisses of the Granite Mountains, Wyoming, in Peterman, Z.E., and Schnabel, D.C. (eds.), Shorter contributions to isotope research: U.S. Geological Survey Bulletin 1622, p. 13-23.

* Fremont County GIS/Map Server and Property information: http://fremontcountywy.org/2012/01/gismap-server/, accessed April 2014.

* Frost, C.D., and Frost, B.R., 1993, The Archean history of the Wyoming province, *in* Snoke, A.W., Steidtmann, J.R., and Roberts, S.M., eds., Geology of Wyoming: Wyoming State Geological Survey Memoir 5, p. 58-76.

Frost, C.D., Frost, B.R., Chamberlain, K.R., and Hulsebosch, T.P., 1998, The Late Archean history of the Wyoming province as recorded by granitic magmatism in the Wind River Range, Wyoming. Precambrian Research, v. 89, p. 145-173.

Frost, C.D., Fruchey, B.L., Chamberlain, K.R., and Frost, R.B., 2006, Archean crustal growth by lateral accretion of juvenile supracrustal belts in the south-central Wyoming Province: Canadian Journal of Earth Sciences, v. 43, p. 1533-1555.

Fruchey, B.L., 2002, Archean supracrustal sequences of contrasting origin- the Archean history of the Barlow Gap area, northern Granite Mountains, Wyoming: Laramie, University of Wyoming, M.S. thesis, 178 p., scale 1:24,000, and 1:3,000.

Grace, R.L.B., Chamberlain, K.R., Frost, B.R., and Frost, C.D., 2006, Tectonic histories of the Paleoarchean to Mesoarchean Sacawee block and Neoarchean Oregon Trail structural belt of south-central Wyoming Province: Canadian Journal of Earth Sciences, v. 43, no. 10, p. 1445-1466.

Hausel, W.D., 1991, Economic geology of the South Pass granite-greenstone belt, southern Wind River Mountains, western Wyoming: Geological Survey of Wyoming [Wyoming State Geological Survey] Report of Investigations 44, 129 p.

Hausel, W.D., 1994, Economic geology of the Seminoe Mountains mining district, Carbon County, Wyoming: Wyoming State Geological Survey Report of Investigations 50, 31 p. scale 1:24,000.

Hausel, W.D., 1996, Geology and gold mineralization of the Rattlesnake Hills, Granite Mountains, Wyoming: Wyoming State Geological Survey Report of Investigations 52, 28 p., scale 1:24,000.

Hausel, W.D., Graff, P.J., and Albert, K.G., 1985, Economic geology of the Copper Mountain supracrustal belt, Owl Creek Mountains, Fremont County, Wyoming: Geological Survey of Wyoming [Wyoming State Geological Survey] Report of Investigations No.28, 33 p., 3 pls, scale 1:24,000.

Houston, R.S., 1983, Wyoming Precambrian Province - example of the evolution of mineral deposits through time? *in* Roberts, S., ed., Metallic and nonmetallic mineral deposits of Wyoming and adjacent areas, 1983 Conference Proceedings: Geological Survey of Wyoming [Wyoming State Geological Survey] Public information Circular 25, p. 1-12.

Kruckenberg, S.C., Chamberlain, K.R., Frost, C.D., and Frost, B.R., 2001, One billion years of Archean crustal evolution: Black Rock Mountain, northeastern Granite Mountains, Wyoming: Geological Society of America Abstracts with Programs, v. 33, no. 6, p. 401.

Langstaff, G.D., 1995, Archean geology of the Granite Mountains: Golden, Colorado School of Mines, Ph.D. dissertation, 671 p., scale 1:24,000.

* Love, J.D., 1961, Split Rock Formation (Miocene) and Moonstone Formation (Pliocene) in central Wyoming: U.S. Geological Survey Bulletin 1121-I, 39 p.

Love, J.D., 1970, Cenozoic geology of the Granite Mountains area, central Wyoming: U.S. Geological Survey Professional Paper 495-C, 154 p., 4 pls, scale 1:125,000.

* Love, J.D., and Christiansen, A.C., 1985, Geologic map of Wyoming: U.S. Geological Survey Map, scale 1:500,000.

Love, J.D., Christiansen, A.C., and Ver Ploeg, A.J., 1993, Stratigraphic chart showing Phanerozoic nomenclature for the State of Wyoming, Wyoming State Geological Survey Map Series 41.

Ludwig, K.R., and Stuckless, J.S., 1978, Uranium-lead isotope systematics and apparent ages of zircons and other minerals in Precambrian granitic rocks, Granite Mountains, Wyoming: Contributions to Mineralogy and Petrology, v. 65, p. 243-254.

* Natrona County GIS/Map Server and Property information: http://geosmart.casperwy.gov/, accessed April 2014.

Peterman, Z.E., and Hildreth, R.A., 1978, Reconnaissance geology and geochronology of the Precambrian of the Granite Mountains, Wyoming: U.S. Geological Survey Professional Paper 1055, 22 p.

Rachou, J.F., 1951, Tertiary stratigraphy of the Rattlesnake Hills, central Wyoming: Laramie, University of Wyoming, M.A. thesis, 70 p.

* Stuckless, J.S., and Peterman, Z.E., 1977, A summary of the geology, geochronology, and geochemistry of Archean rocks of the Granite Mountains, Wyoming: Wyoming Geological Association Earth Science Bulletin, v. 10(3), p. 3-20.

Sutherland, W.M., Gregory, R.W., Carnes, J.D., and Worman, B.N., 2013, Rare Earth Elements in Wyoming: Wyoming State Geological Survey Report of Investigations No. 65, 82 p.

Sutherland, W.M., and Hausel, W.D., 2003, Geologic Map of the Rattlesnake Hills 30' x 60' quadrangle, Fremont and Natrona Counties, Wyoming: Wyoming State Geological Survey Map Series 61, 28 p., scale 1:100,000.

Sutherland, W.M., and Hausel, W.D., 2005, Geologic map of the Barlow Gap quadrangle, Natrona County, Wyoming: Wyoming State Geological Survey Map Series 67, scale 1:24,000.

Sutherland, W.M., and Worman, B.N., 2013, Preliminary geologic map of the Blackjack Ranch quadrangle, Natrona County, Wyoming: Wyoming State Geological Survey Open File Report 13-3, 24 p., scale 1:24,000.

Van Houten, F.B., 1955, Volcanic-rich Middle and Upper Eocene sedimentary rocks northwest of Rattlesnake Hills central Wyoming: U.S. Geological Survey Professional Paper 274-A, 14 p.

Van Houten, F.B., 1964, Tertiary geology of the Beaver Rim area Fremont and Natrona Counties, Wyoming: U.S. Geological Survey Bulletin 1164, 99 p., 8 pls, scale 1:62,500.

WOGCC, 2014, Wyoming Oil and Gas Conservation Committee website, at http://wogcc.state.wy.us/, accessed May 2014.

Appendix I
Petrographic Analysis

Sample S1: 20140506LC-B
Hand sample: White quartzite in Agna near sheared contact with Ash
Mineralogy: Quartz, Plagioclase, Biotite
Petrographic Description: Quartz is major component and exhibits crystal deformation with patchwork extinction. Biotite exhibits sweeping extinction and optical continuity in separated grains indicating dissolution has occurred. A foliation is not apparent. Plagioclase is not common but twinning is evident in few grains.

Sample S2: 20140507WS-A
Hand sample: Altered ultramafic or volcanic (Xd/Ad)
Mineralogy: Serpentine, Feldspar, Olivine, Opaques, Cordierite, Sericite
Petrographic Description: Olivine is present as cracked crystals with a serpentine alteration rim. Serpentine is also seen as radiating with sweeping extinction and no preferred orientation. Feldspar is sericitized in part and deformed. Opaques are scattered throughout. Small blebs of cordierite are pseudomorphed by sericite and serpentine.

Sample S3: 20140507LC-A
Hand sample: Altered ultramafic or volcanic (Xd/Ad)
Mineralogy: Serpentine, Diopside, Tremolite, Orthopyroxene, Olivine, Cordierite, Opaques
Petrographic Description: Serpentine is present as acicular and sweeping grains throughout. Diopside is common as large partially dissolved grains with optical continuity. The diopside and serpentine are most likely responsible for the green coloration in hand sample. Tremolite and orthopyroxene are also present. Chromite hypothetically makes up the opaques based on elevated chromium in this sample. Small, grey blebs with yellow inclusions are identified as cordierite replaced by serpentine along the rim.

Sample S4: 20140507LC-B
Hand sample: Altered ultramafic or volcanic (Xd/Ad)
Mineralogy: Serpentine, Olivine, Cordierite, Rutile, Sericite
Petrographic Description: Olivine grains are cracked and rounded with a serpentine alteration rim. Cordierite grains are anhedral, small, and are also replaced by sericite and serpentine. Cordierite is identified by its smooth, low-relief, grayish color in XPL and very clear/bright white in PPL.

Sample S5: 20140508WS-A
Hand sample: Green quartzite from Bullet Hill (Agna)
Mineralogy: Quartz, Serpentine, Cordierite, Muscovite
Petrographic Description: Quartz is amoeboid and has patchwork extinction indicating deformation. Serpentine and muscovite appear foliated, blocky, and sucrosic indicating multiple growth generations. The foliation is created during times of localized strain, but the sucrosic and blocky textures crystallize during isostatic pressure. When cordierite is seen it is almost entirely replaced by serpentine and only present as tiny blebs.

Sample S6: 20140508LC-A
Hand Sample: Altered ultramafic or volcanic (Xd/Ad)
Mineralogy: Plagioclase, Quartz, Serpentine, Biotite, Olivine, Rutile, Cordierite
Petrographic Description: Biotite is present as coarse, euhedral grains and not in a foliation. Olivine is cracked, rounded, and partially replaced by fibrous serpentine. Serpentine also occurs in two orientations. Plagioclase and quartz are both very anhedral.

Sample S7: 20140508LC-B
Hand Sample: Sheared ultramafic or volcanic (Xd/Ad)
Mineralogy: Biotite, Serpentine, Monazite, Cordierite
Petrographic Description: Multiple generations of biotite, some with preferred orientation in the foliation and some cross cutting perpendicular. Serpentine is radiating and grains appear bent around cordierite blebs as a possible replacement texture. The same biotite texture is observed around possible monazites which appear subrounded with pleochroic halos.

Sample S8: 20140520LC-A
Hand sample: Amphibolite (Xd/Ad)
Mineralogy: Gedrite, Quartz, Plagioclase, Biotite, Rutile, Cordierite, Kyanite
Petrographic Description: Quartz exhibits patchwork extinction. Gedrite is acicular and radiating with sweeping extinction. Cordierite and kyanite appear as anhedral inclusions within quartz and plagioclase grains.

Sample S9: 20140520LC-B
Hand Sample: Blue-grey quartzite used for radiometric dating (Agna)
Mineralogy: Quartz, Cordierite (replacing Staurolite), Biotite, Serpentine, Sillimanite
Petrographic Description: Patchwork quartz with blocky slightly oriented biotite. Granular and fibrous serpentine throughout composes reaction rims on cordierite blebs. Cordierite appears to have shape similar to the habit of staurolite in cross section. This implies that the original mineral may have been staurolite and was psedudomorphed to cordierite. In some grains, clear, unoriented needles are observed and identified as sillimanite.

Sample S10: 20140521LC-A
Hand sample: Gt-rich amphibolite (Abs)
Mineralogy: Hornblende, Actinolite, Garnet (Pyrope-Almandine), Quartz, Sericite, opaques
Petrographic Description: Garnet in the rock has a pyrope-almandine composition and contains quartz, amphibole, and opaque inclusions. The garnet also preserves an earlier texture where amphibole grains and inclusion paths of opaques are oriented differently from the current foliation (S1 foliation). Subhedral hornblende and actinolite are both present and form a strong, continuous foliation (S2 foliation) until intersecting garnet. The amphiboles appear to bend around the garnet porphyroblasts indicating the current amphibole foliation (S2) crystallized post garnet growth. The amphibole and garnet grains are partially replaced on edges by sericite.

Sample S11: 20140521LC-C
Hand Sample: Felsite (Agna)
Mineralogy: K-feldspar, Quartz, Fe-oxide stain, Muscovite
Petrographic Description: K-feldspar is present as large grains with tartan twinning, sweeping extinction, myrmekitic texture. Quartz exhibits patchwork extinction. These textures indicate dissolution and crystal deformation occurred. Muscovite is minor and very anhedral.

Sample S12: 20140528WS-A
Hand Sample: Blue-gray quartzite (Agna)
Mineralogy: Quartz, Serpentine, Sericite, Cordierite (very very small amounts)
Petrographic Description: Large patchwork quartz grains with annealed fractures indicate the occurrence of deformation. Serpentine is swirling, unoriented, and possibly replacing cordierite, which is present as small blebs throughout.

Sample S13: 20140528LC-A
Hand sample: Granitic Gneiss (Agna?)
Mineralogy: K-feldspar, Plagioclase, Quartz, Chlorite, Fe-oxidation
Petrographic Description: Feldspars preserve rock deformation in the form of deformation twins, kinking, sweeping extinction, myrmekitic texture, broken/annealed grains, and offset fractures. Chlorite creates a weak, discontinuous foliation.

Sample S14: 20140529WS-A
Hand sample: Red gneiss/pegmatite (Argn)
Mineralogy: K-feldspar, Quartz, Chlorite, Opaques, Fe-staining, Monazite/Zircon
Petrographic Description: K-feldspar and quartz grains are anhedral. Chlorite forms a foliation and partially dissolved grains exhibit optical continuity. Opaques are scattered throughout as well as minerals with pleochroic halos assumed to be a type of monazite or zircon.

Sample S15: 20140530WS-A
Hand sample: Agna orthogneiss for radiometric dating
Mineralogy: K-feldspar, Plagioclase, Quartz, Biotite
Petrographic Description: Biotite creates a spaced, discontinuous foliation with poor preferred orientation. Optical continuity of grains indicates partial dissolution. Sweeping extinction in feldspars as well as patchwork extinction in quartz indicates deformation. Vermicular texture along quartz-feldspar grain boundaries indicates either exsolution of feldspars during cooling or metasomatic replacement during deformation.

Sample S16: 20140530WS-B
Hand sample: Brown dike (Xd/Ad)
Mineralogy: Plagioclase, Opaques, Chlorite, Muscovite, Fe-staining
Petrographic Description: Very fine-grained with no preferred orientation. Iron oxide staining contributes to the brown, fuzzy coloration and texture.

Appendix II
Geochronologic Evaluation of Sample 20140530WS-A

Sample Collection Location: Lat. 42.667836, Long. -107.534327
Collected by Wayne M. Sutherland and Elizabeth C. Cola on May 30, 2014
Rock unit: Antler orthogneiss

Report on U-Pb date of the Antler Granite, Granite Mountains, Wyoming.

Kevin R. Chamberlain, Research Professor, University of Wyoming, September 5, 2014.

Zircon grains were separated by standard crushing and mineral separation methods. The recovered zircons had a range of morphologies from extra-large and euhedral (Figure 1) to short and stubby (Figure 2). All populations were extremely metamict. Grains were subdivided into 4 morphologies for processing: 1) exlarge, euhedral, 2) large and elongate, 3) short and stubby, 4) anhedral. Very few grains from each population survived the first step of CA-TIMS dissolution; data come from the short and stubby population, but the range of ages indicate that this is not a single population.

Selected zircons were annealed at 850 °C for 50 hours, then dissolved in two steps in a chemical abrasion, thermal ionization mass spectrometric U-Pb dating method (CATIMS) modified from Mattinson (2005). The first dissolution step was in hydrofluoric acid (HF) and nitric acid (HNO3) at 180 °C for 12 hours. This removed the most metamict zircon domains in the annealed crystals. Individual grains were then spiked with a mixed 205Pb-233U-235U tracer (ET535), completely dissolved in HF and HNO3 at 240 °C for 30 hours, and then converted to chlorides. The dissolutions were loaded onto rhenium filaments with phosphoric acid and silica gel without any further chemical processing. Pb and UO2 isotopic compositions were determined in single Dalyphotomultiplier mode on a Micromass Sector 54 mass spectrometer. Data were reduced and ages calculated using PbMacDat and ISOPLOT/EX after Ludwig (1988, 1991).

Eight single grain analyses produced concordant or nearly concordant data that do not overlap within error (Figure 3, Table 1). 207Pb/206Pb dates range from ca 3320 to 3380 Ma (Figure 4). Th/U values from all are similar and are consistent with magmatic growth. Data are interpreted to reflect magmatism ca. 3325 Ma or younger, with inherited components as old as 3372 Ma.

Figure 1. Extra-large zircons from Antler granite sample 20140530WS-A. Note the high degree of metamictization.

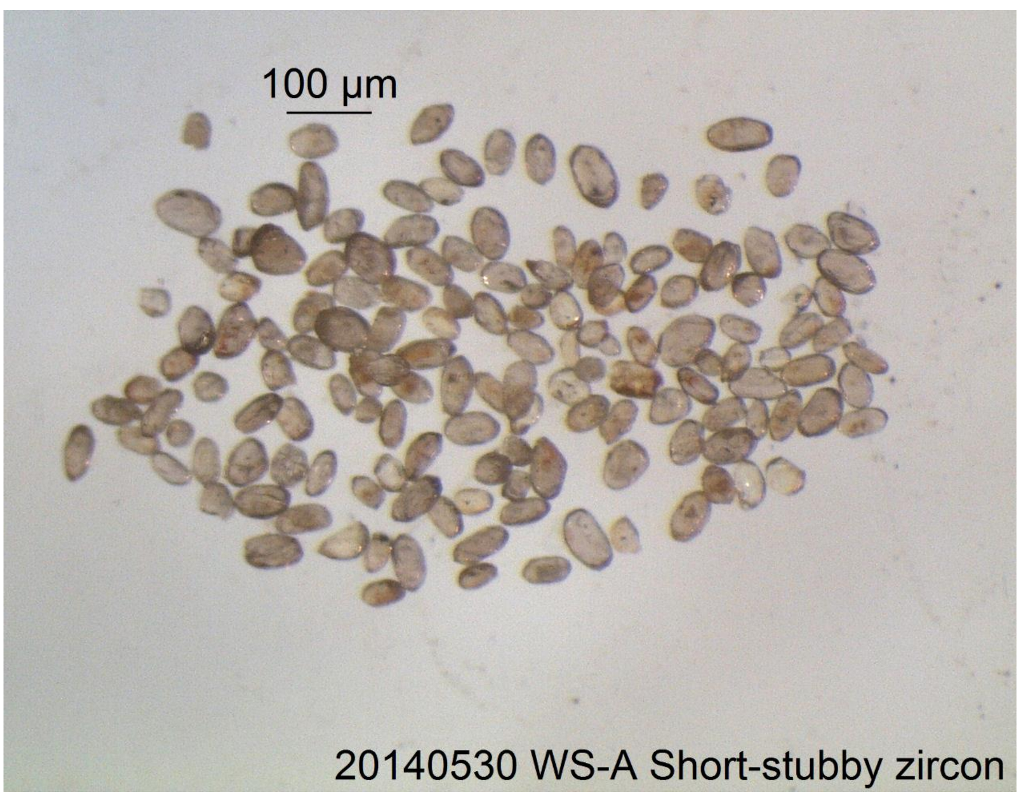

Figure 2. Examples of short and stubby zircons isolated from Antler granite sample. This subpopulation had the highest survival rate from the first step of dissolution (10%). All the CA-

TIMS data come from this population, yet the variation in ages indicates that they are not a single growth population.

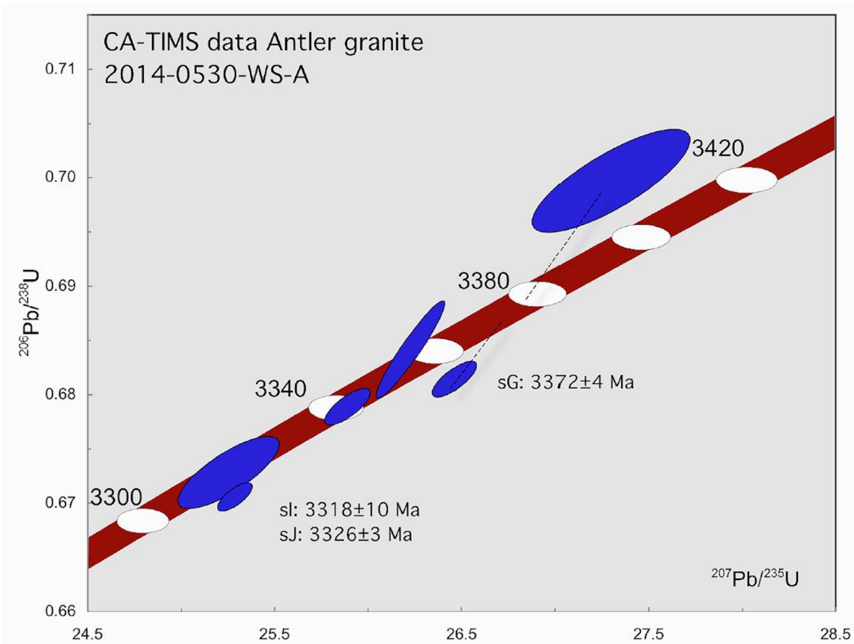

Figure 3. U-Pb zircon data from single grain CA-TIMS analyses from 20140530WS-A. Decay constant errors are included to display Concordia as a swath. Although each analysis is concordant or nearly so, they display a range of 207Pb/206Pb dates and do not overlap within error. Data are interpreted to reflect magmatism ca. 3325 Ma with inheritance as old as 3372 Ma.

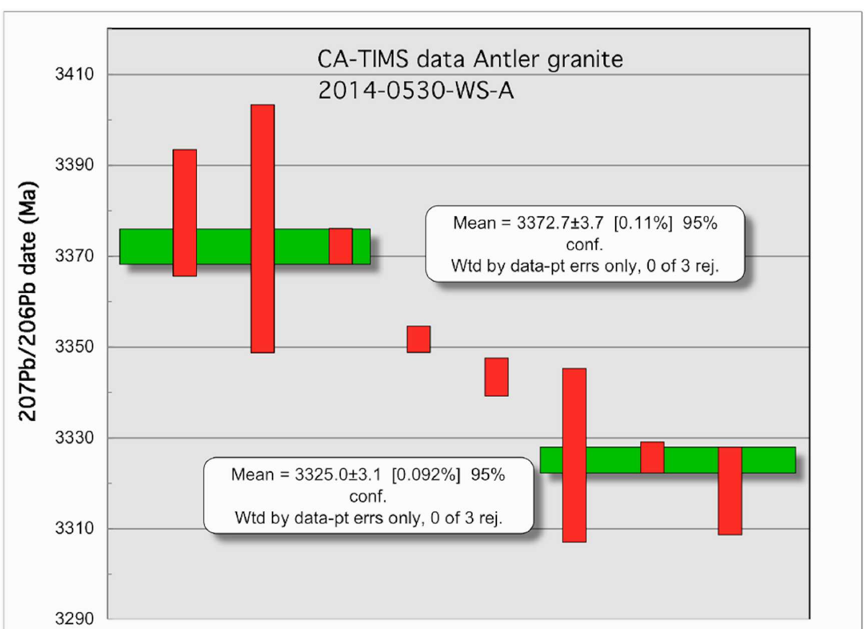

Figure 4. Plot of $^{207}Pb/^{206}Pb$ dates from single zircon analyses of the Antler granite. The data are interpreted to reflect magmatism ca. 3325 Ma or more recently with inheritance as old as 3373 Ma.

References (including table 1):

Krogh, T.E., 1973, A low-contamination method for hydrothermal decomposition of zircon and extraction of U and Pb for isotopic age determinations: Geochimica et Cosmochimica Acta, v. 37, p. 485–494.

Ludwig, K.R., l988, PBDAT for MS-DOS, a computer program for IBM-PC compatibles for processing raw Pb-U-Th isotope data, version 1.24: U.S. Geological Survey, Open-File Report 88-542, 32 pp.

Ludwig, K.R., l991, ISOPLOT for MS-DOS, a plotting and regression program for radiogenic-isotope data, for IBM-PC compatible computers, version 2.75: U.S. Geological Survey, Open-File Report 91-445, 45 pp.

Ludwig, K. R., 1998, On the treatment of concordant uranium-lead ages. Geochimica et Cosmochimica Acta, 62(4), 665-676.

Mattinson, J.M, 2005, Zircon U-Pb chemical abrasion ("CA-TIMS") method: combined annealing and multi-step partial dissolution analysis for improved precision and accuracy of zircon ages: Chemical Geology, v. 220, p. 47-66.

Parrish, R.R., Roddick, J.C., Loveridge, W.D., and Sullivan, R.D., l987, Uranium-lead analytical techniques at the geochronology laboratory, Geological Survey of Canada, in Radiogenic age and isotopic studies, Report 1: Geological Survey of Canada Paper 87-2, p. 3–7.

Stacey, J.S. and Kramers, J.D., 1975, Approximation of terrestrial lead isotope evolution by a two-stage model: Earth and Planetary Science Letters, v. 26, p. 207–221.

Steiger, R.H. and Jäger, E., 1977, Subcommission on geochronology: convention on the use of decay constants in geo- and cosmochronology: Earth and Planetary Science Letters, v. 36, p. 359–362.

Table 1 U-Pb CATIMS zircon data

Sample	Weight (µg)	U (ppm)	sample Pb (ppm)	sample Pb (pg)	TcPb (pg)	Th/U	Pb*/Pbc	206Pb/204Pb	206Pb/208Pb	Corrected atomic ratios: 206Pb/238U (rad.)	%err	207Pb/235U (rad.)	%err	207Pb/206Pb (rad.)	%err	206/238 Age (Ma)	207/235 Age (Ma)	207/206 Age (Ma)	err	Rho	% disc.
2014-0530-WS-A Antler granite (42.667836, -107.534327)										*crystallization age = 3343 Ma or younger with inheritance 3372 Ma or older*											
sF	0.70	119	105	74	8.5	0.40	8.0	381	9.46	0.6842	(0.53)	26.2250	(0.57)	0.2780	(0.19)	3360.5	3355.0	3351.6	±2.9	0.95	-0.34
sG	0.12	399	326	38	2.7	0.42	14.0	762	8.96	0.6815	(0.20)	26.4639	(0.37)	0.2816	(0.25)	3350.1	3363.8	3372.0	±3.9	0.76	0.84
sA	0.29	167	136	39	2.9	0.45	13.5	734	8.36	0.6790	(0.20)	25.8894	(0.39)	0.2765	(0.27)	3340.6	3342.4	3343.4	±4.2	0.76	0.11
sI	0.04	491	383	14	2.6	0.28	5.4	313	13.25	0.6730	(0.40)	25.2508	(0.88)	0.2721	(0.61)	3317.3	3318.0	3318.4	±9.6	0.78	0.04
sJ	0.04	637	498	18	1.0	0.30	18.1	1005	12.38	0.6707	(0.16)	25.2847	(0.30)	0.2734	(0.21)	3308.6	3319.3	3325.8	±3.4	0.74	0.66
sM	0.01	742	632	6	3.1	0.45	1.8	111	8.36	0.6889	(4.21)	26.8173	(4.65)	0.2823	(1.74)	3378.3	3376.8	3375.9	±27	0.93	-0.09
sL	0.02	294	258	6	1.5	0.66	3.8	211	5.78	0.6997	(0.55)	27.3009	(1.26)	0.2830	(0.89)	3419.6	3394.3	3379.4	±14	0.80	-1.53
sH	0.13	162	137	17	7.1	0.34	2.3	137	10.99	0.6766	(2.83)	25.5138	(3.24)	0.2735	(1.22)	3331.2	3328.1	3326.2	±19	0.93	-0.19

Notes: sample: s_=single grain
Weight: represents estimated weight after first step of CATIMS dissolution. U and Pb concentrations are based on this weight and may be over-estimations depending on how much material was dissolved and leached in the first step. Picograms (pg) sample and initial Pb from the second dissolution step are measured directly.
sample Pb: sample Pb (radiogenic + initial) corrected for laboratory blank
TcPb: total common Pb. Blank was 3 pg or less. All greater than 3 pg was assigned to initial Pb.
Pb*/Pbc: radiogenic Pb to total common Pb (blank + initial)
Corrected atomic ratios: $^{206}Pb/^{204}Pb$ corrected for mass discrimination and tracer, all others corrected for blank, mass discrimination, tracer and initial Pb, values in parentheses are 2 sigma errors in percent.
Rho: $^{206}Pb/^{238}U$ vs $^{207}Pb/^{235}U$ error correlation coefficient
% disc.: percent discordant

Zircon dissolution and chemistry were adapted from methods developed by Krogh (1973), Parrish et al. (1987) and Mattinson (2005). All zircons were chemically abraded (CATIMS). Final dissolutions were spiked with a mixed $^{205}Pb/^{233}U/^{235}U$ tracer (ET535). Pb and U samples were loaded onto single rhenium filaments with silica gel.
Isotopic compositions were measured in single Daly mode Micromass Sector 54 mass spectrometer at the University of Wyoming.
Mass discrimination of 0.247 ± 0.10 %/amu for Pb was determined by replicate analyses
of NIST SRM 981. U fractionation was determined internally during each run. Procedural blanks averaged 3 pg Pb during the course of the study. Isotopic composition of the Pb blank was measured as 18.851±1.2, 15.665±0.75, and 38.188±1.2 for 206/204, 207/204 and 208/204, respectively. U blanks were consistently less than 0.1 pg. Concordia coordinates, intercepts, and uncertainties were calculated using MacPBDAT and ISOPLOT programs (based on Ludwig 1988, 1991); initial Pb isotopic compositions were estimated by Stacey and Kramers (1975) model. The decay constants used by MacPBDAT are those recommended by the I.U.G.S. Subcommission on Geochronology (Steiger and Jäger, 1977): 0.155125 x 10^{-9}/yr for ^{238}U, 0.98485 x 10^{-9}/yr for ^{235}U and present-day $^{238}U/^{235}U$ = 137.88.

Appendix III
Geochronologic Evaluation of Sample 20140520LC-B

Sample Collection Location: Lat. 42.65618, Long. -107.574690
Collected by Wayne M. Sutherland and Elizabeth C. Cola on May 30, 2014
Rock unit: Bluish-black quartzite within the Antler orthogneiss

Report on LA-ICP-MC-MS dating of detrital zircons from 2014-0520 LC-B.

Kevin Chamberlain, Research Professor, University of Wyoming, July 20, 2014.

Zircons were separated by standard crushing and concentration methods. Minimal magnetic filtering was applied to minimize bias in the zircon population. A wide range of zircon sizes was recovered, from ≥800 to ≤50 microns in length (Figure 1). Extra-large grains were mounted on a separate slide so that they could be polished to their centers without losing smaller grains. A representative population of zircons were mounted on two slides (22 large and extra-large, approximately 150 medium to small grains) and analyzed by Laser Ablation Inductively Coupled Plasma Multicollector Mass Spectrometry (LA-ICP-MC-MS) at the University of California at Santa Barbara by John Cottle. 57 spots on the large grains and 144 spots on the small grains were analyzed. Many of the analyses were reversely discordant with 206Pb/238U dates that are older than their 207Pb/206Pb dates. This characteristic is commonly observed with Archean, metamict zircons analyzed by laser and may reflect a mis-match between ablation rates in relatively undamaged standards and metamict zircons. The 206Pb/238U dates are less reliable in this situation and only the 207Pb/206Pb dates are interpreted. Results are presented in Table 1, plotted on Concordia in Figure 2 and as Probability Distribution plots in Figure 3 & 4. Data from two spots, large #29 and small #121, were excluded as their 207Pb/206Pb dates are too young and are inconsistent with field relations that require deposition circa 2.85 Ga.

Age distribution is heavily concentrated ca. 3.3 Ga, the age of the basal Sacawee and related gneisses, with lesser peaks ca. 3.1 Ga and 2.90 Ga, the ages of other intrusions in the Barlow Gap area (Grace et al., 2006). Youngest grains are ca. 2.86 Ga (large #24, small #49, 50, 103, 108), one grain is 3.5 Ga (small #135).

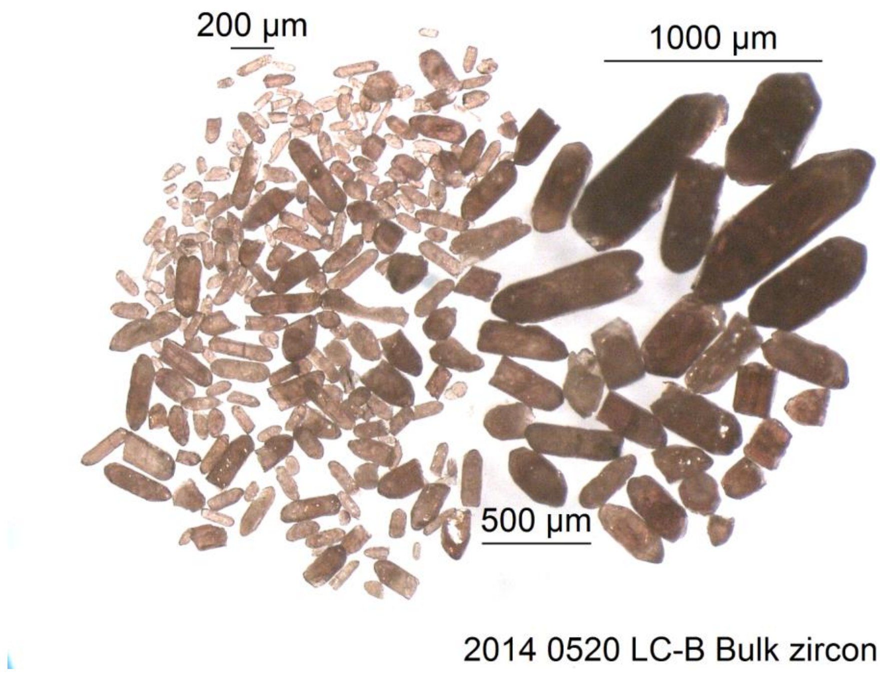

Figure 1. Representative zircons from 20140520LC-B. Large and extra-large grains were mounted separately so that they could be polished to their centers for LA-ICP analysis.

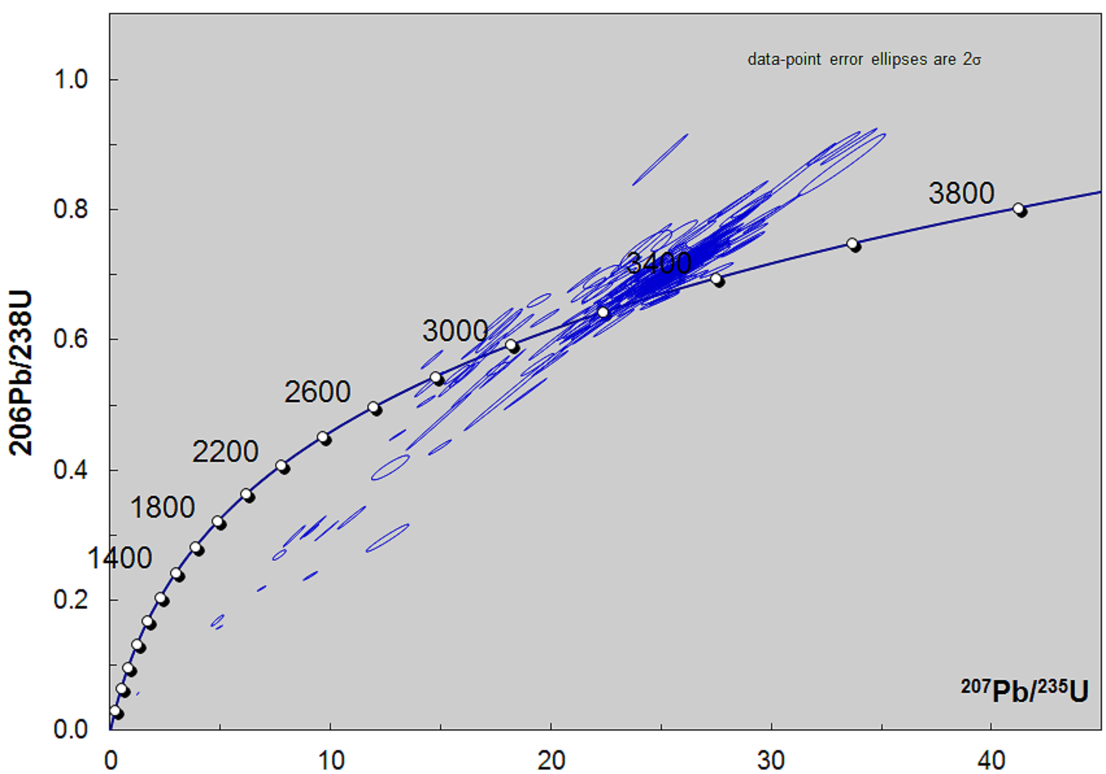

Figure 2. LA-ICP data from all spots from 20140520LC-B. Due to the metamict nature of these Archean grains, the U vs Pb downhole fractionation was not well matched by standards so some of the discordance may be analytical artifacts. The 207Pb/206Pb dates are reliable however.

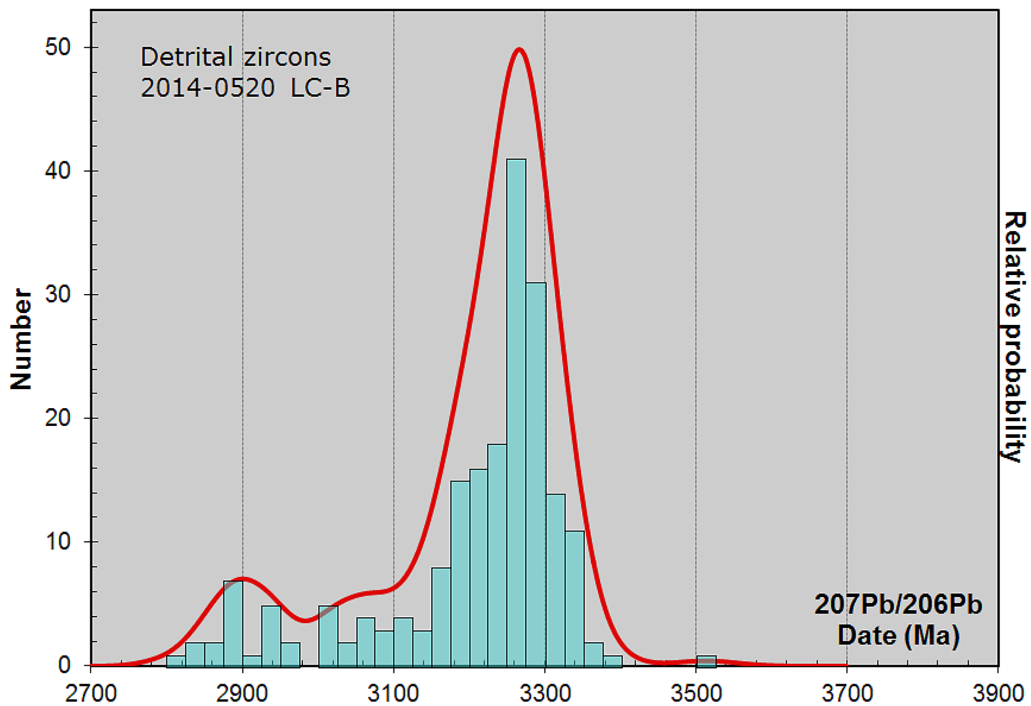

Figure 3. Probability density plot of age spectrum from all data from detrital zircons from 20140520LC-B. Major peak is ca. 3.3 Ga, with minor peaks at 3.1 and 2.9 Ga. All 3 are ages of plutons in the region and represent basement at the time of deposition.

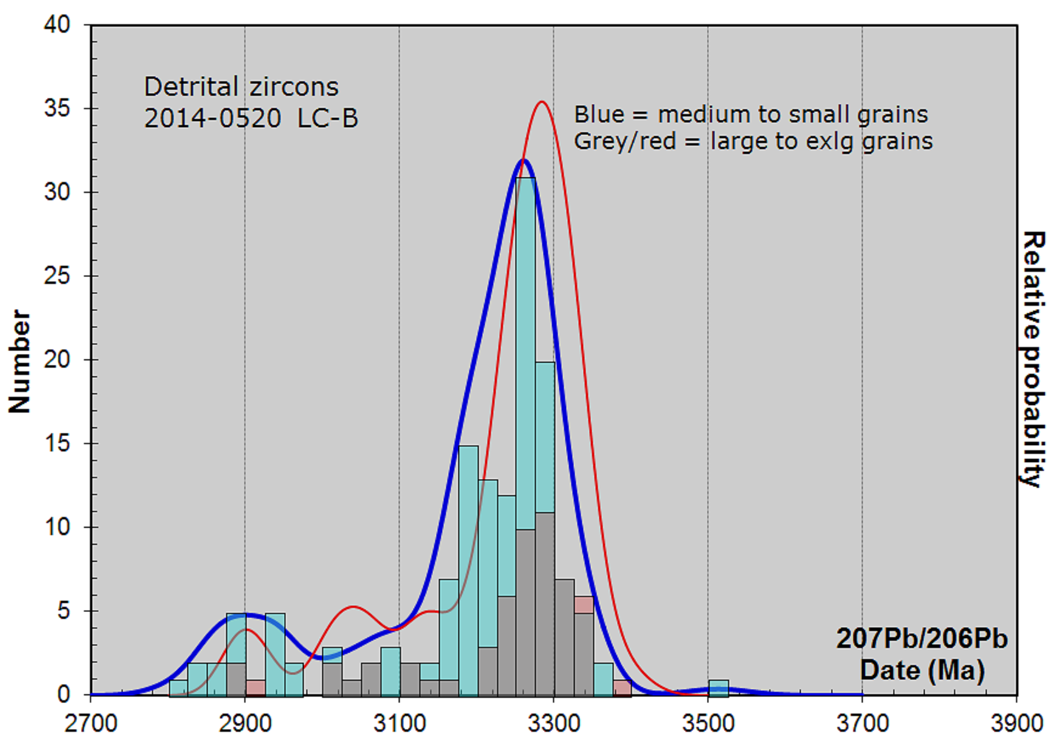

Figure 4. Probability plot of detrital zircon 207Pb/206Pb dates separated by size. The same peaks are represented by both sub-populations, with a slight shift toward older dates in the larger grains.

Table 1

Sample name	Pb (ppm)	U (ppm	Th (ppm)	Th/U	207/206	2s. %	207/235	2s. %	206/238	2s. %	Rho	207/206 Age	2s. Abs.	206/238 Age	2s. Abs.
520LCB_large_1	221	196	38	0.19	0.2719	1.81	26.410	2.28	0.6955	1.39	0.98	3317	60	3408	47
520LCB_large_2	908	533	166	0.31	0.2688	1.82	25.290	2.45	0.6789	1.65	0.99	3299	60	3350	55
520LCB_large_3	535	461	101.3	0.22	0.2737	1.81	25.150	2.18	0.6635	1.23	0.98	3327	60	3280	40
520LCB_large_4	443	389	85.2	0.22	0.2732	1.81	24.710	2.22	0.6569	1.29	0.98	3324	60	3254	42
520LCB_large_5	402.4	367.8	76.5	0.21	0.2750	1.80	25.160	2.20	0.6661	1.25	0.98	3335	60	3290	41
520LCB_large_6	427	370	80.6	0.22	0.2719	1.81	24.760	2.20	0.6642	1.25	0.95	3317	60	3284	41
520LCB_large_7	166	132	28.6	0.21	0.2713	1.83	26.120	2.41	0.7038	1.58	0.97	3314	61	3434	54
520LCB_large_8	557	428	101.2	0.23	0.2712	1.81	25.480	2.22	0.6877	1.29	0.98	3313	60	3373	43
520LCB_large_9	544	451	102.7	0.22	0.2738	1.81	25.420	2.19	0.6810	1.23	0.97	3328	60	3347	41
520LCB_large_10	196	179	33.5	0.18	0.2764	1.81	27.090	2.30	0.7201	1.41	0.98	3342	61	3498	49
520LCB_large_11	640	519	116	0.23	0.2721	1.82	18.840	4.22	0.5170	3.81	1.00	3318	60	2678	102
520LCB_large_12	3020	2940	1074	0.37	0.2311	1.81	6.864	2.30	0.2183	1.42	0.97	3060	56	1273	18
520LCB_large_13	1021	910	260	0.28	0.2539	1.84	14.960	2.82	0.4352	2.13	0.98	3209	59	2329	50
520LCB_large_14	1010	564	164.3	0.29	0.2769	1.81	29.430	2.73	0.7860	2.04	0.99	3346	61	3739	76
520LCB_large_15	245.9	119.9	45.7	0.38	0.2858	1.81	27.520	2.25	0.7070	1.34	0.97	3395	62	3448	46
520LCB_large_16	509	455	111.8	0.25	0.2557	1.81	21.200	2.32	0.6105	1.45	0.99	3220	58	3076	45
520LCB_large_17	2080	1015	398	0.39	0.2692	1.80	25.840	2.16	0.7057	1.19	0.99	3301	60	3442	41
520LCB_large_18	156	113.4	22.2	0.19	0.2737	1.84	28.790	2.70	0.7670	1.97	0.98	3327	61	3668	72
520LCB_large_19	333	300	58.5	0.20	0.2684	1.81	25.930	2.17	0.7096	1.21	0.96	3296	60	3456	42
520LCB_large_20	1041	772	194.2	0.26	0.2649	1.80	25.220	2.15	0.6955	1.18	0.98	3276	59	3405	40
520LCB_large_21	1692	1168	308.8	0.27	0.2677	1.80	26.280	2.18	0.7170	1.23	0.99	3293	59	3484	43
520LCB_large_22	3620	1072	593	0.56	0.2404	1.83	23.380	2.59	0.7120	1.84	0.99	3122	57	3463	64
520LCB_large_23	253	382	44.5	0.12	0.2631	1.82	25.660	2.18	0.7112	1.21	0.93	3265	59	3462	42
520LCB_large_24	1870	666	24.1	0.03	0.2075	1.82	24.960	4.10	0.8770	3.67	1.00	2886	52	4050	149
520LCB_large_25	1484	893	277.7	0.31	0.2665	1.80	25.930	2.14	0.7072	1.16	0.98	3286	59	3449	40
520LCB_large_26	546	430	101.9	0.24	0.2660	1.80	25.510	2.26	0.6998	1.36	0.99	3283	59	3421	47
520LCB_large_27	244	245	38.2	0.15	0.2690	1.84	27.300	2.57	0.7330	1.80	0.97	3300	61	3551	64
520LCB_large_28	1316	762	205.3	0.27	0.2624	1.81	26.580	2.48	0.7310	1.69	0.99	3261	59	3537	60
520LCB_large_29	1631	4100	2660	0.65	0.1602	1.91	1.243	3.41	0.0567	2.83	0.98	2457	47	355	10
520LCB_large_30	5660	2460	1515	0.61	0.2091	1.80	13.040	2.32	0.4541	1.46	0.99	2898	52	2416	35
520LCB_large_31	238.2	228.6	44.6	0.19	0.2617	1.81	25.100	2.28	0.6981	1.39	0.98	3257	59	3414	47
520LCB_large_32	1693	1184	311	0.26	0.2589	1.81	22.900	2.40	0.6408	1.58	0.98	3240	59	3191	50
520LCB_large_33	104.4	148.8	22	0.14	0.2610	1.87	28.840	3.37	0.8010	2.81	0.98	3252	61	3788	106
520LCB_large_34	387	351	66	0.19	0.2688	1.81	26.760	2.24	0.7250	1.32	0.98	3299	60	3516	47
520LCB_large_35	2337	1377	439	0.32	0.2633	1.80	25.520	2.19	0.7056	1.23	0.97	3267	59	3441	42
520LCB_large_36	649.3	527.9	115.3	0.22	0.2638	1.80	25.680	2.18	0.7092	1.22	0.99	3270	59	3455	42
520LCB_large_37	422	435.7	80.1	0.18	0.2469	1.81	22.550	2.18	0.6657	1.22	0.97	3165	57	3289	40
520LCB_large_38	774	429	131	0.28	0.2662	1.81	26.050	2.20	0.7125	1.26	0.98	3284	59	3467	44
520LCB_large_39	393.1	350.5	71.3	0.21	0.2658	1.81	25.440	2.19	0.6986	1.24	0.98	3282	59	3415	42
520LCB_large_40	476.3	354.8	93.3	0.26	0.2537	1.80	23.260	2.16	0.6652	1.18	0.97	3208	58	3287	39
520LCB_large_41	523	303	87.7	0.31	0.2579	1.82	19.960	3.37	0.5640	2.84	1.00	3234	59	2878	82
520LCB_large_42	237	231.9	36.3	0.15	0.2679	1.81	25.870	2.21	0.7007	1.25	0.94	3294	60	3422	43
520LCB_large_43	1053	695	194	0.27	0.2645	1.80	25.640	2.21	0.7033	1.27	0.99	3274	59	3435	44
520LCB_large_44	4360	1760	713	0.41	0.2406	1.82	23.240	2.32	0.6986	1.44	0.98	3124	57	3414	49
520LCB_large_45	2453	1155	478	0.43	0.2259	2.01	19.720	2.69	0.6336	1.79	0.99	3021	61	3161	57
520LCB_large_46	193	399	86.7	0.21	0.2438	1.92	10.950	4.80	0.3270	4.40	0.99	3144	60	1818	80
520LCB_large_47	1305	721	201	0.28	0.2322	1.82	17.810	4.79	0.5560	4.43	1.00	3067	56	2840	126
520LCB_large_48	1408	801	211	0.26	0.2635	1.81	25.380	2.50	0.6937	1.72	0.99	3267	59	3395	58
520LCB_large_49	299	342	58.1	0.17	0.2639	1.81	24.730	2.25	0.6779	1.35	0.98	3270	59	3337	45
520LCB_large_50	268.8	248.8	52.7	0.21	0.2613	1.81	24.480	2.22	0.6769	1.28	0.95	3254	59	3331	43
520LCB_large_51	585	704	107.3	0.15	0.2590	1.80	24.740	2.17	0.6900	1.20	0.98	3240	58	3382	41
520LCB_large_52	703	1230	115.2	0.09	0.2270	1.92	17.600	2.43	0.5559	1.48	0.86	3033	58	2849	42
520LCB_large_53	465	450	66.8	0.15	0.2576	1.82	25.990	2.49	0.7280	1.70	0.98	3232	59	3524	60
520LCB_large_54	3820	3890	1690	0.44	0.2237	1.82	4.947	2.34	0.1587	1.47	0.97	3007	55	949	14
520LCB_large_55	2400	1204	448	0.36	0.2580	1.83	24.770	2.54	0.6940	1.75	0.98	3234	59	3395	60
520LCB_large_56	1418	1176	173	0.15	0.2124	1.83	19.450	2.24	0.6607	1.29	0.90	2924	54	3269	42
520LCB_large_57	306.7	875	55.7	0.06	0.2602	1.80	25.320	2.18	0.7026	1.22	0.97	3248	59	3430	42

z520LCBsmall_1	844	607	340	0.55	0.2779	1.85	9.080	2.92	0.2377	2.25	0.98	3351	62	1374	31
z520LCBsmall_2	394	611	65	0.11	0.2638	1.83	25.550	2.17	0.7039	1.16	0.98	3270	60	3435	40
z520LCBsmall_3	473	573	43.3	0.07	0.2706	1.82	26.920	3.56	0.7250	3.06	1.00	3310	60	3510	108
z520LCBsmall_4	598	294	78.7	0.26	0.2652	1.86	26.810	2.66	0.7380	1.91	0.98	3278	61	3573	68
z520LCBsmall_5	570	425	90	0.21	0.2668	1.85	25.940	3.19	0.7070	2.60	1.00	3287	61	3446	90
z520LCBsmall_6	315	331	53.3	0.16	0.2662	1.81	25.990	2.28	0.7117	1.38	0.99	3284	59	3464	48
z520LCBsmall_7	338	286	56.1	0.20	0.2552	1.85	22.360	3.05	0.6350	2.42	0.99	3217	60	3166	77
z520LCBsmall_8	506	1690	97.2	0.06	0.2130	1.90	17.330	3.32	0.5910	2.73	0.99	2930	56	2992	82
z520LCBsmall_9	964	1814	313	0.17	0.2145	2.49	9.200	5.23	0.3120	4.60	1.00	2937	73	1748	80
z520LCBsmall_10	375	332	68	0.20	0.2665	1.86	24.720	3.63	0.6770	3.12	1.00	3287	61	3329	104
z520LCBsmall_11	510	498	97	0.16	0.2676	1.99	26.060	2.98	0.7110	2.21	0.96	3292	66	3459	76
z520LCBsmall_12	518	812	107.2	0.13	0.2506	1.82	21.250	2.73	0.6180	2.04	0.99	3188	58	3100	63
z520LCBsmall_13	181.1	195.5	34.6	0.17	0.2736	1.82	25.900	2.19	0.6898	1.21	0.93	3327	61	3382	41
z520LCBsmall_14	575	1090	97.9	0.09	0.2174	1.83	18.520	3.07	0.6210	2.47	0.99	2961	54	3112	77
z520LCBsmall_15	233.4	270.3	42	0.15	0.2600	1.82	24.290	2.17	0.6804	1.19	0.92	3247	59	3346	40
z520LCBsmall_16	2960	1290	680	0.52	0.2064	1.86	14.330	2.37	0.5055	1.46	0.98	2877	54	2637	39
z520LCBsmall_17	2088	1112	356	0.32	0.2491	2.02	22.910	2.79	0.6690	1.92	0.88	3178	64	3302	64
z520LCBsmall_18	337	542	65.5	0.12	0.2476	1.84	21.290	3.95	0.6260	3.50	0.99	3169	58	3132	110
z520LCBsmall_19	382.9	359.6	69.6	0.19	0.2652	1.82	24.880	2.82	0.6830	2.15	0.99	3278	60	3354	72
z520LCBsmall_20	965	707	182	0.25	0.2560	1.83	23.810	2.74	0.6760	2.04	0.99	3222	59	3337	68
z520LCBsmall_21	260	403	30.5	0.08	0.2643	1.82	26.920	3.41	0.7400	2.88	1.00	3273	59	3571	103
z520LCBsmall_22	1579	481.2	249.6	0.52	0.2790	1.81	28.560	2.54	0.7440	1.78	1.00	3358	61	3585	64
z520LCBsmall_23	308	427	37.3	0.09	0.2692	1.82	27.740	2.70	0.7540	1.99	0.99	3301	60	3620	72
z520LCBsmall_24	505	1073	88.8	0.08	0.2649	1.80	26.080	2.57	0.7160	1.83	1.00	3276	59	3479	64
z520LCBsmall_25	254	301	30.2	0.10	0.2674	1.86	26.440	3.72	0.7190	3.22	0.99	3291	61	3491	112
z520LCBsmall_26	118.3	505	20.3	0.03	0.2620	1.81	26.590	3.19	0.7410	2.63	1.00	3259	59	3570	94
z520LCBsmall_27	184	362	27.2	0.07	0.2532	1.85	26.530	2.97	0.7620	2.33	0.98	3205	59	3649	85
z520LCBsmall_28	1737	1051	266	0.25	0.2501	1.84	25.250	2.94	0.7290	2.29	0.97	3185	59	3529	81
z520LCBsmall_29	391	827	72	0.08	0.2368	1.86	22.700	4.69	0.6920	4.31	0.99	3099	58	3380	146
z520LCBsmall_30	1483	381	260.7	0.67	0.2659	2.01	26.560	3.05	0.7260	2.30	0.95	3281	66	3515	81
z520LCBsmall_31	1170	710	191	0.25	0.2585	1.84	24.580	2.72	0.6920	2.00	0.98	3238	60	3391	68
z520LCBsmall_32	4650	2090	964	0.46	0.2090	1.90	15.730	2.94	0.5470	2.25	0.97	2898	55	2823	63
z520LCBsmall_33	2030	1230	367	0.29	0.2267	2.07	16.800	6.40	0.5360	6.05	1.00	3029	63	2760	167
z520LCBsmall_34	1730	913	249	0.27	0.2641	1.85	29.090	2.58	0.8050	1.80	0.97	3271	60	3806	68
z520LCBsmall_35	217.2	913	37.8	0.04	0.2677	1.80	26.140	2.75	0.7140	2.08	1.00	3292	59	3471	72
z520LCBsmall_36	548	953	81.2	0.08	0.2705	1.80	26.920	2.39	0.7245	1.57	1.00	3309	60	3512	55
z520LCBsmall_37	241.3	640	39.5	0.06	0.2664	1.81	26.290	2.66	0.7190	1.95	0.99	3285	59	3491	68
z520LCBsmall_38	392	592	63	0.11	0.2520	1.81	24.450	2.76	0.7070	2.09	1.00	3197	58	3445	72
z520LCBsmall_39	906	536	133.2	0.25	0.2640	1.81	28.170	2.82	0.7800	2.17	1.00	3271	59	3716	81
z520LCBsmall_40	2080	921	354	0.38	0.2606	1.81	25.590	3.05	0.7150	2.45	1.00	3250	59	3476	85
z520LCBsmall_41	323.6	377	31.5	0.08	0.2698	1.82	26.420	3.60	0.7130	3.11	1.00	3305	60	3469	108
z520LCBsmall_42	365.8	240.4	58.7	0.24	0.2636	1.84	25.540	2.98	0.7060	2.35	0.99	3268	60	3442	81
z520LCBsmall_43	634	382	79.5	0.21	0.2584	1.82	24.880	2.98	0.7020	2.36	0.99	3237	59	3427	81
z520LCBsmall_44	535	761	78.4	0.10	0.2668	1.82	23.890	2.98	0.6550	2.36	0.99	3287	60	3245	77
z520LCBsmall_45	1415	805	257	0.32	0.2673	1.82	27.300	2.90	0.7410	2.26	0.99	3290	60	3583	81
z520LCBsmall_46	235	560	30.6	0.05	0.2587	1.81	26.230	2.90	0.7380	2.27	1.00	3239	59	3562	81
z520LCBsmall_47	1080	837	165	0.18	0.2555	2.09	25.440	3.02	0.7230	2.18	0.92	3218	67	3507	76
z520LCBsmall_48	303	388.5	58.4	0.15	0.2549	1.85	22.030	4.09	0.6280	3.64	1.00	3216	60	3142	114

Sample name	Pb (ppm)	U (ppm	Th (ppm)	Th/U	207/206	2s. %	207/235	2s. %	206/238	2s. %	Rho	207/206 Age	2s. Abs.	206/238 Age	2s. Abs.
z520LCBsmall_49	2.40E+04	2370	7250	2.93	0.1974	2.29	14.480	3.77	0.5320	2.99	0.99	2803	64	2747	82
z520LCBsmall_50	1369	2920	196.5	0.07	0.2051	2.15	7.670	3.17	0.2699	2.34	0.86	2866	62	1540	36
z520LCBsmall_51	2009	470	312	0.66	0.2749	1.81	30.040	3.56	0.7940	3.06	1.00	3334	60	3762	115
z520LCBsmall_52	1142	793	201.5	0.25	0.2551	1.87	24.420	2.74	0.6950	2.00	0.97	3217	60	3400	68
z520LCBsmall_53	421	364	57.3	0.16	0.2640	1.87	27.300	3.01	0.7500	2.36	0.99	3271	61	3607	85
z520LCBsmall_54	196	465	27	0.06	0.2647	1.82	27.360	3.18	0.7500	2.60	0.99	3275	60	3620	94
z520LCBsmall_55	427.2	1237	75.9	0.06	0.2409	1.85	22.100	2.57	0.6730	1.79	0.94	3126	58	3315	59
z520LCBsmall_56	1090	850	188	0.22	0.2504	1.88	23.040	3.43	0.6690	2.87	0.97	3187	60	3299	95
z520LCBsmall_57	1080	703	176	0.25	0.2545	1.89	25.300	2.88	0.7260	2.17	0.96	3213	61	3516	76
z520LCBsmall_58	450	1264	52.4	0.04	0.2088	1.83	17.910	3.31	0.6220	2.76	0.99	2897	53	3118	86
z520LCBsmall_59	64.9	137.6	11.5	0.08	0.2565	1.84	24.370	3.24	0.6880	2.67	0.98	3225	59	3375	90
z520LCBsmall_60	1731	488	272	0.55	0.2692	1.85	27.180	2.84	0.7340	2.15	0.98	3301	61	3546	76
z520LCBsmall_61	1050	579	218	0.37	0.2450	1.83	22.570	3.90	0.6680	3.44	1.00	3152	58	3297	113
z520LCBsmall_62	136.4	170.4	25.2	0.15	0.2682	1.90	26.600	4.69	0.7200	4.28	0.99	3296	62	3490	150
z520LCBsmall_63	748	400	84.5	0.21	0.2637	1.82	30.700	5.94	0.8440	5.66	1.00	3269	60	3940	223
z520LCBsmall_64	1663	1025	310.2	0.30	0.2493	1.84	22.830	2.67	0.6650	1.93	0.98	3180	59	3286	64
z520LCBsmall_65	828	812	154.3	0.19	0.2619	1.89	24.850	2.94	0.6920	2.26	0.96	3258	62	3387	76
z520LCBsmall_66	2630	770	352	0.45	0.2733	1.82	33.520	3.13	0.8970	2.55	0.99	3325	61	4127	105
z520LCBsmall_67	1190	543	164	0.30	0.2776	1.94	33.200	4.89	0.8690	4.49	0.98	3349	65	4030	181
z520LCBsmall_68	901	316.6	145.3	0.45	0.2757	1.82	28.920	2.61	0.7620	1.87	0.99	3339	61	3651	68
z520LCBsmall_69	387	372	65.9	0.18	0.2611	1.81	25.990	2.84	0.7230	2.18	0.99	3254	59	3504	76
z520LCBsmall_70	345	530	62.9	0.12	0.2612	1.81	25.240	2.59	0.7020	1.86	1.00	3254	59	3427	64
z520LCBsmall_71	424	416	34.4	0.08	0.2647	1.84	22.850	3.30	0.6260	2.74	0.99	3275	60	3132	86
z520LCBsmall_72	241	672	35.4	0.05	0.2502	2.12	23.750	3.52	0.6870	2.80	0.98	3185	68	3368	94
z520LCBsmall_73	1321	1075	275	0.25	0.2583	1.81	21.930	3.45	0.6160	2.94	1.00	3237	59	3095	91
z520LCBsmall_74	1311	860	237	0.27	0.2478	1.90	23.480	2.96	0.6870	2.27	0.98	3172	60	3368	76
z520LCBsmall_75	840	597	175	0.27	0.2637	1.82	25.580	4.12	0.7030	3.69	1.00	3269	60	3428	127
z520LCBsmall_76	306	285	47.9	0.17	0.2512	1.83	24.700	3.05	0.7170	2.45	0.99	3192	58	3484	85
z520LCBsmall_77	540	722	54.7	0.07	0.2083	1.98	17.640	4.92	0.6140	4.51	0.99	2892	57	3090	139
z520LCBsmall_78	1066	585	174.2	0.29	0.2620	1.81	27.150	2.61	0.7510	1.88	1.00	3259	59	3611	68
z520LCBsmall_79	296	1406	50.1	0.04	0.2335	1.85	21.700	2.95	0.6770	2.30	0.98	3076	57	3331	77
z520LCBsmall_80	933.6	607	146.2	0.24	0.2500	1.84	24.360	3.41	0.7080	2.86	0.98	3185	59	3450	99

Sample name	Pb (ppm)	U (ppm	Th (ppm)	Th/U	207/206	2s. %	207/235	2s. %	206/238	2s. %	Rho	207/206 Age	2s. Abs.	206/238 Age	2s. Abs.
z520LCBsmall_81	697	560	132.2	0.23	0.2555	1.82	24.410	3.00	0.6940	2.38	0.99	3219	58	3397	81
z520LCBsmall_82	1794	1095	303	0.27	0.2252	1.81	21.500	2.90	0.6920	2.26	0.99	3018	55	3388	76
z520LCBsmall_83	319.9	366.3	51.6	0.14	0.2648	1.82	26.240	2.94	0.7180	2.32	0.99	3275	60	3488	81
z520LCBsmall_84	2220	1350	381	0.28	0.2310	2.12	22.280	3.00	0.6970	2.12	0.89	3059	65	3410	72
z520LCBsmall_85	1078	743	189.2	0.25	0.2606	1.81	25.880	3.14	0.7180	2.57	1.00	3250	59	3487	90
z520LCBsmall_86	157	268	20.6	0.08	0.2641	1.87	32.830	3.00	0.8940	2.35	0.99	3271	61	4136	97
z520LCBsmall_87	182.5	296	31.1	0.10	0.2460	2.17	25.600	3.37	0.7600	2.57	0.95	3159	69	3665	94
z520LCBsmall_88	486	794	36.7	0.04	0.2352	1.84	24.100	4.68	0.7400	4.31	0.99	3088	57	3570	154
z520LCBsmall_89	499	502	80.8	0.16	0.2629	1.82	27.000	3.20	0.7410	2.63	1.00	3264	60	3571	94
z520LCBsmall_90	641	649	96.1	0.15	0.2542	1.82	21.570	4.29	0.6120	3.89	1.00	3211	59	3076	120
z520LCBsmall_91	387.7	1126	84	0.07	0.2519	2.27	18.400	10.38	0.5260	10.13	1.00	3197	73	2720	275
z520LCBsmall_92	1650	1101	394	0.32	0.2028	1.81	16.500	2.79	0.5860	2.13	1.00	2849	51	2974	63
z520LCBsmall_93	168.4	916	38.4	0.04	0.2135	1.89	15.720	4.29	0.5380	3.85	0.99	2932	55	2774	107
z520LCBsmall_94	253	401	47.4	0.12	0.2631	1.82	25.900	3.50	0.7100	2.99	0.99	3266	59	3456	103
z520LCBsmall_95	321	261.7	55	0.21	0.2663	1.82	26.840	2.65	0.7290	1.93	0.99	3284	60	3528	68
z520LCBsmall_96	147	117.4	25.3	0.20	0.2680	1.86	26.870	3.71	0.7230	3.20	0.98	3295	61	3507	112
z520LCBsmall_97	1286	674	199	0.29	0.2607	1.81	28.350	3.19	0.7820	2.63	1.00	3251	59	3724	98
z520LCBsmall_98	2210	1320	399	0.30	0.2466	1.89	23.990	3.57	0.7000	3.03	0.99	3163	60	3419	103
z520LCBsmall_99	1106	354	193.8	0.54	0.2764	1.82	28.720	2.80	0.7470	2.12	0.99	3342	61	3595	76
z520LCBsmall_100	731	803	143.2	0.18	0.2567	1.81	24.390	3.02	0.6830	2.41	1.00	3227	58	3354	81
z520LCBsmall_101	936	825	203	0.24	0.2503	1.80	22.790	3.31	0.6550	2.78	1.00	3186	57	3245	90
z520LCBsmall_102	372	1000	72	0.07	0.2261	3.89	12.710	5.47	0.4040	3.85	0.90	3022	118	2186	84
z520LCBsmall_103	455	1640	129	0.08	0.2066	2.28	4.860	4.73	0.1692	4.14	0.94	2878	66	1007	42
z520LCBsmall_104	107.4	137.7	15.3	0.11	0.2504	1.91	22.720	3.38	0.6530	2.79	0.97	3187	61	3239	90
z520LCBsmall_105	523	312	76	0.19	0.2593	1.87	28.010	3.55	0.7730	3.02	0.99	3242	61	3688	111
z520LCBsmall_106	385	652	47.9	0.07	0.2495	1.81	21.100	2.74	0.6090	2.06	1.00	3181	58	3065	63
z520LCBsmall_107	213	720	37.7	0.06	0.2594	1.82	24.310	3.04	0.6750	2.44	1.00	3243	59	3325	81
z520LCBsmall_108	820	1040	148	0.14	0.2015	1.91	8.350	4.85	0.2990	4.46	0.99	2838	54	1683	75
z520LCBsmall_109	152.3	370	28	0.07	0.2687	1.81	26.610	2.66	0.7160	1.95	0.99	3298	60	3481	68
z520LCBsmall_110	391	753	75.6	0.10	0.2595	1.81	24.600	2.53	0.6820	1.77	0.99	3244	59	3358	60
z520LCBsmall_111	269.9	561	52.1	0.09	0.2628	1.81	25.280	2.60	0.6950	1.87	0.99	3263	59	3400	64
z520LCBsmall_112	488	330.1	85.8	0.26	0.2613	1.81	26.610	2.90	0.7360	2.27	0.99	3255	59	3554	81
z520LCBsmall_113	337.7	256.2	56.2	0.22	0.2522	1.83	22.700	3.46	0.6510	2.94	0.99	3198	58	3230	95
z520LCBsmall_114	2275	1317	400	0.30	0.2466	1.83	23.990	2.98	0.7030	2.36	0.99	3163	58	3430	81
z520LCBsmall_115	2280	1380	678	0.48	0.2246	2.69	14.900	8.11	0.4750	7.64	1.00	3017	81	2490	190
z520LCBsmall_116	1033	761	190	0.24	0.2584	1.82	25.530	3.05	0.7140	2.45	0.99	3237	59	3473	85
z520LCBsmall_117	301	719	52.2	0.07	0.2651	1.81	27.810	2.77	0.7600	2.10	1.00	3277	59	3643	76
z520LCBsmall_118	322	209.4	51.6	0.25	0.2723	1.84	26.990	3.48	0.7180	2.96	0.99	3319	61	3487	103
z520LCBsmall_119	1580	1089	295	0.27	0.2612	1.81	25.150	2.78	0.6980	2.11	0.99	3254	59	3411	72
z520LCBsmall_120	1160	876	218	0.24	0.2613	1.81	25.070	3.00	0.6910	2.39	1.00	3255	59	3405	81
z520LCBsmall_121	237	1381	43.5	0.03	0.1857	1.82	14.600	2.72	0.5700	2.02	0.99	2705	49	2905	59
z520LCBsmall_122	478	456	74.9	0.16	0.2616	1.82	28.050	2.75	0.7760	2.06	0.99	3257	59	3712	77
z520LCBsmall_123	820	840	155	0.17	0.2051	1.86	17.610	3.07	0.6300	2.44	0.99	2867	53	3150	77
z520LCBsmall_124	141.2	146	26.1	0.17	0.2608	1.82	25.100	3.53	0.7010	3.02	0.99	3251	59	3422	103
z520LCBsmall_125	401	324	68.9	0.21	0.2545	1.81	24.670	2.77	0.7070	2.09	0.99	3213	58	3446	72
z520LCBsmall_126	288	706	62.2	0.09	0.2441	1.86	20.040	4.25	0.5970	3.82	0.99	3147	58	3017	115
z520LCBsmall_127	228.8	297	41.8	0.14	0.2608	1.84	23.750	3.31	0.6620	2.76	0.99	3251	60	3275	90
z520LCBsmall_128	221	804	43	0.05	0.2610	1.82	25.220	3.52	0.7030	3.02	1.00	3253	59	3426	103
z520LCBsmall_129	222	305	40.9	0.14	0.2650	1.81	25.490	2.49	0.6989	1.70	0.99	3277	59	3416	58
z520LCBsmall_130	276	1342	53.4	0.04	0.2529	1.80	23.670	2.62	0.6800	1.90	1.00	3203	58	3344	64
z520LCBsmall_131	907	727	172	0.24	0.2636	1.81	25.450	2.97	0.7020	2.36	1.00	3268	59	3425	81
z520LCBsmall_132	381	314	42.9	0.14	0.2541	1.84	28.170	3.07	0.8050	2.45	0.99	3210	59	3806	93
z520LCBsmall_133	367	807	85.8	0.11	0.2508	1.88	19.380	3.15	0.5620	2.52	0.98	3190	60	2873	72
z520LCBsmall_134	450	574	37.1	0.07	0.2177	1.94	16.650	4.93	0.5660	4.53	0.99	2963	58	2890	131
z520LCBsmall_135	2180	2150	474	0.22	0.3088	2.40	12.580	6.30	0.2960	5.83	0.97	3513	84	1666	97
z520LCBsmall_136	630	671	94	0.09	0.2386	2.38	24.320	3.93	0.7400	3.14	0.85	3109	74	3582	112
z520LCBsmall_137	333	640	49.7	0.08	0.2613	1.82	26.200	2.65	0.7280	1.93	0.98	3254	59	3523	68
z520LCBsmall_138	1053	635	141	0.23	0.2571	1.84	28.700	3.31	0.8170	2.76	1.00	3229	59	3872	107
z520LCBsmall_139	3430	1300	569	0.44	0.2322	1.81	9.820	4.42	0.3070	4.03	1.00	3067	56	1724	70
z520LCBsmall_140	561	515	47	0.09	0.2480	1.85	26.530	3.66	0.7670	3.16	0.99	3172	59	3670	116
z520LCBsmall_141	1350	2422	549	0.23	0.2144	1.85	9.110	3.10	0.3071	2.49	0.98	2939	54	1726	43
z520LCBsmall_142	521	1921	105.1	0.05	0.2400	1.81	21.180	2.54	0.6378	1.78	0.99	3120	56	3179	57
z520LCBsmall_143	420	881	79.4	0.09	0.2125	1.87	16.070	3.47	0.5470	2.92	0.98	2925	55	2812	82
z520LCBsmall_144	443	1008	83.8	0.08	0.2562	1.81	24.880	2.68	0.7010	1.98	1.00	3223	58	3424	68